ARTICLE Communicated by Bard Ermentrout

Asynchronous States and the Emergence of Synchrony in Large Networks of Interacting Excitatory and Inhibitory Neurons

D. Hansel
David.Hansel@biomedicale.univ-paris5.fr
Laboratoire de Neurophysique et de Physiologie du Système Moteur, Université René Descartes, 75270 Paris Cedex 06, France, and Interdisciplinary Center for Neural Computation, Hebrew University of Jerusalem, 91904 Jerusalem, Israel

G. Mato
matog@cab.cnea.gov.ar
Comisión Nacional de Energía Atómica and CONICET, Centro Atómico Bariloche and Instituto Balseiro (CNEA and UNC), 8400 San Carlos de Bariloche, R.N., Argentina

We investigate theoretically the conditions for the emergence of synchronous activity in large networks, consisting of two populations of extensively connected neurons, one excitatory and one inhibitory. The neurons are modeled with quadratic integrate-and-fire dynamics, which provide a very good approximation for the subthreshold behavior of a large class of neurons. In addition to their synaptic recurrent inputs, the neurons receive a tonic external input that varies from neuron to neuron. Because of its relative simplicity, this model can be studied analytically. We investigate the stability of the asynchronous state (AS) of the network with given average firing rates of the two populations. First, we show that the AS can remain stable even if the synaptic couplings are strong. Then we investigate the conditions under which this state can be destabilized. We show that this can happen in four generic ways. The first is a saddle-node bifurcation, which leads to another state with different average firing rates. This bifurcation, which occurs for strong enough recurrent excitation, does not correspond to the emergence of synchrony. In contrast, in the three other instability mechanisms, Hopf bifurcations, which correspond to the emergence of oscillatory synchronous activity, occur. We show that these mechanisms can be differentiated by the firing patterns they generate and their dependence on the mutual interactions of the inhibitory neurons and cross talk between the two populations. We also show that besides these codimension 1 bifurcations, the system can display several codimension 2 bifurcations: Takens-Bogdanov, Gavrielov-Guckenheimer, and double Hopf bifurcations.

1 Introduction

Synchrony can be defined in several ways. In its broader definition, the activities of two neurons are said to be synchronized if some kind of temporal correlations exist between them. In this sense, in any system of interacting neurons, some level of synchrony should exist. In this respect, observing synchrony between directly interacting neurons should not be surprising. In fact, several studies in the 1960s and 1970s were devoted to determining what the shape of the cross-correlations of a pair of neurons can tell us about their interactions (Abeles, 1990). The implicit assumption in this approach was that correlations are dominated by direct interactions between the neurons.

Other types of synchronous states can emerge through cooperative effects. In these states, the correlations in the activity of a pair of neurons in the network depend weakly on their direct interaction (Hansel & Sompolinsky, 1996). Instead, they are mostly mediated by the inputs to the neurons coming from all other neurons belonging to the part of the network with which they interact. To define this type of synchronous state, it is appropriate to consider macroscopic observables, for example, the instantaneous activity of the neurons averaged across assemblies of neurons (multi-unit activities) or local field potentials that presumably reflect electrical activity induced by many neurons. In an asynchronous state, the temporal fluctuations of these quantities (suitably normalized) are small—on the order of $1/M$ where M is the size of the neuronal assembly. When synchrony emerges, these fluctuations become finite even if the population is large. Understanding the conditions for the emergence of these states in the brain is one of the goals of recent research in the field of collective neuronal dynamics. Central issues concern the roles of the cellular properties of the neurons; the nature (excitatory, inhibitory), the strength, and the kinetics of the synaptic interactions; and the local and global architectures of the networks. The ways in which noise, heterogeneities, and spatial fluctuations of connectivity patterns affect synchrony are also among the fundamental questions investigated. One possible approach to these questions is to study cooperative dynamical states in simplified network models of local neuronal populations in the brain. Within limits, these models can be studied in depth analytically. Subsequently, these analytical investigations can be extended using numerical simulations beyond the limits that can be treated analytically. This approach has led to substantial progress in our understanding of the general mechanisms of neuronal synchrony. However, most of the theoretical studies have addressed the case of one population of neurons, much less is known about networks comprising several populations.

The goal of this article is to study the emergence of synchronous activity in large networks consisting of two interacting populations of neurons, one excitatory and the other inhibitory. We investigate the conditions

under which asynchronous states (AS) become unstable due to interactions. More specifically, we inquire: (1) Under which conditions can the network display a stable asynchronous state? Is this possible when the couplings are strong? (2) What are the different mechanisms through which the AS can become unstable in the network? (3) In what ways do they depend on the recurrent interactions in the excitatory neurons, the mutual interactions of the inhibitory neurons, and the excitatory-inhibitory feedback connections between the two populations? (4) What patterns of synchrony emerge when the AS is unstable? In particular, can one differentiate unambiguously between the regimes of parameters in which neurons spike in synchrony from regimes in which they burst in synchrony? (5) More quantitatively, what determines the period of the synchronous oscillations and the phase shift between the oscillations in the two populations?

The article is organized as follows. The model is introduced in section 2. In section 3, the method of AS stability analysis is presented, and a spectral equation for the eigenmodes of the linearized dynamics is established. Assuming that the synaptic time constants of the excitatory and inhibitory synapses are identical simplifies the analysis of this equation. This allows us in section 4 to study the instabilities of AS to a large extent completely analytically. The various bifurcations of the AS are characterized. The results of section 4 are subsequently generalized in section 5. Results from numerical simulations are presented in section 6. Section 7 is devoted to a discussion of our results.

2 The model

2.1 The Quadratic Integrate-and-Fire Model. Near the onset of firing, it can be shown that the detailed dynamics of any type I conductance-based model can be replaced by the reduced model (Ermentrout & Kopell, 1986; Ermentrout, 1996),

$$\bar{C}\frac{dV}{dt} = A\left(V - V^\star\right)^2 + I - I_c, \tag{2.1}$$

where I_c is the rheobase of the neuron. Analytical formulas can be derived to compute the effective capacitance $\bar{C}$, the constant A, and $V^\star$. Using these formulas, one can compute these parameters numerically as functions of the biophysical parameters of the full conductance-based model (see appendixes A and B). The solution of equation 2.1 diverges in finite time. This divergence corresponds to the firing of an action potential. If one supplements equation 2.1 with the condition that the variable V has to be reset to $-\infty$ following a spike, this yields a reduced model that accurately describes the dynamics of the full conductance-based model in the limit $I \to I_c$. In

this model, the relationship between the firing rate ν and the current I is given by

$$\nu = B\sqrt{I - I_c}, \tag{2.2}$$

where $B = \sqrt{A}/\pi\bar{C}$.

When $I - I_c$ is not small, this reduction is no longer exact. However, one can generalize it heuristically as follows. We assume that action potentials are fired whenever V crosses some threshold, V_t (from below), and that it is immediately reset to a value V_r. The relationship between the discharge rate and the external current of the model is now given by

$$\frac{1}{\nu} = \frac{1}{\pi B}\frac{\arctan(\frac{V_t\sqrt{A}}{\sqrt{I-I_c}}) - \arctan(\frac{V_r\sqrt{A}}{\sqrt{I-I_c}})}{\sqrt{I - I_c}}. \tag{2.3}$$

The two parameters, V_t and V_r, are phenomenological. They are not determined by the exact reduction method near the firing onset, and additional constraints are required to determine them. In the following, we impose that the $\nu - I$ curve of the quadratic integrate-and-fire (QIF) model matches the $\nu - I$ curve of the full model as much as possible.

It is convenient to rewrite the reduced model in terms of the dimensionless variables $\bar{V}$ and $\bar{I}$ defined by

$$\bar{V} = \frac{A}{\bar{C}}\tau_0(V - V^\star) \tag{2.4}$$

$$\bar{I} = \frac{A}{\bar{C}^2}I\tau_0^2, \tag{2.5}$$

where τ_0 has a dimension of a time. The dynamics are governed by

$$\tau_0\frac{d\bar{V}}{dt} = \bar{V}^2 + \bar{I} - \bar{I}_c. \tag{2.6}$$

The dynamical variable $\bar{V}$ is reset to $\bar{V}_r = A(V_r - V^\star)\tau_0/\bar{C}$ whenever it reaches the threshold value: $\bar{V}_t = A(V_t - V^\star)\tau_0/\bar{C}$. A similar model has been used by Latham, Richmond, Nelson, and Nirenberg (2000) to study with numerical simulations a two-population network model.

In this article, we use a QIF model with parameters derived from the Wang-Buszaki (WB) conductance-based model described in appendix A. Using the approach described above, one finds that $I_c = 0.1601$ mA/cm^2, $V^\star = -59.5462$ mV, $\bar{C} = 0.9467$ μF/cm^2, and $A = 0.012875$ mS/cm^2/mV. Requiring that the ν-I curve of the reduced and the full model agrees well up to firing rates as large as $\nu_{\max} = 100$ spikes per second yields for the other parameters $V_r - V^\star = -4.6$ mV and $V_t - V^\star = 33.2$ mV ($\bar{V}_r = -0.626$,

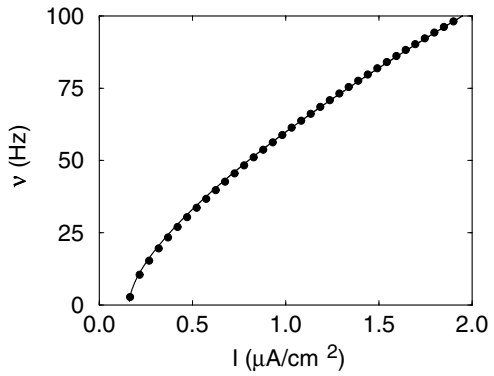

Figure 1: Firing rate of a neuron versus the external current. Circles: Wang-Buszáki model. Solid line: QIF model with $A = 0.012875$ mS/cm^2/mV, $V_r - V^* = -4.6$ mV, $V_t - V^* = 33.2$ mV, $I_c = 0.1601$ muA/cm^2 and $\bar{C} = 0.9467$ μF/cm^2.

$\bar{V}_t = 4.52$). The ν-I curves of the full model and the QIF model with these parameters are plotted in Figure 1. Clearly the fit is excellent over a broad range of firing rates.

The traces of the membrane potential for neurons firing at 50 spikes per second and 10 spikes per second are shown in Figures 2A and 2B, respectively, for this QIF model. For comparison, we have also plotted the traces of a WB neuron that fires at the same frequencies. For a frequency of 10 Hz, the traces are very similar. When the frequency increases, the traces of the QIF neuron deviate from those of the WB neuron.

2.2 The Two-Population Network Model. We deal with a network of two heterogeneous populations: one excitatory and the other inhibitory. The dynamics of the neurons is modeled by equation 2.6,

$$\frac{dV_{i\alpha}}{dt} = V_{i\alpha}^2 + I_{i\alpha} + I_{i\alpha}^{syn}(t) - I_\alpha^{th} \tag{2.7}$$

where $i = 1, \ldots, N_\alpha$ are the indices of the neurons in population α ($\alpha = E, I$). For simplicity, the firing threshold of the neurons V_t, the resetting value V_r, and the rheobase currents are the same for all the neurons. Time is measured in units of $\tau_0 = 10$ ms. The current $I_{i\alpha}$ represents the effect of an external stimulus that is assumed to be constant in time but different from one neuron to another.

We consider the case where N_α is very large and the external input currents to the neurons in population α are distributed according to a density distribution $Q_\alpha(I)$. The synaptic current, $I_{i\alpha}^{syn}(t)$, on the ith cell, is the sum of

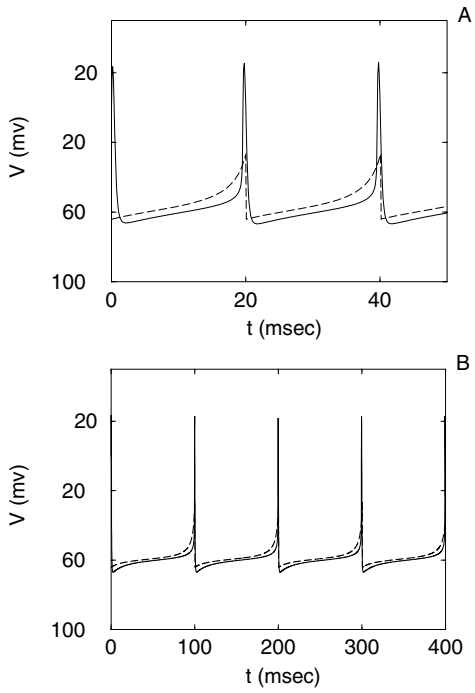

Figure 2: Traces of a WB neuron (solid line) and QIF neuron (dashed line). Parameters of the model are the same as in Figure 1. (A) The neuron fires at 50 Hz. (B) The neuron fires at 10 Hz.

all contributions $I^{syn}_{ij\alpha\beta}$ from all the presynaptic cells on it:

$$I^{syn}_{i\alpha}(t) = \sum_{j\beta} I^{syn}_{ij\alpha\beta}(t). \tag{2.8}$$

In this work, the current $I^{syn}_{ij\alpha\beta}(t)$ is modeled by

$$I^{syn}_{ij\alpha\beta}(t) = G^{syn}_{ij\alpha\beta}\, s_{j\beta}(t), \tag{2.9}$$

where $G^{syn}_{ij\alpha\beta}$ measures the strength of the synapses that neuron j in population β makes on neuron i in population α and $s_{j\beta}$ evolves with time according to

$$s_{j\beta}(t) = \sum_{\text{spikes}} f_\beta(t - t_{\text{spike,j}}), \tag{2.10}$$

where the summation is performed over all the spikes emitted by the presynaptic neuron with an index j at times $t_{\mathrm{spike,j}}$. The function $f_\beta(t)$ is

$$f_\beta(t) = \frac{1}{\tau_{2\beta} - \tau_{1\beta}} \left[\exp\left(-\frac{t}{\tau_{1\beta}}\right) - \exp\left(-\frac{t}{\tau_{2\beta}}\right) \right] \Theta(t). \tag{2.11}$$

Here, $\Theta(t)$ is the Heaviside function, and the normalization is such that the integral of $f_\beta(t)$ is one.

The characteristic times $\tau_{1\beta}$ and $\tau_{2\beta}$ are the rise and decay times of the synapse, respectively. In case $\tau_{1\beta} = \tau_{2\beta} = \tau_\beta$, one obtains the so-called alpha function (Rall, 1967):

$$f_\beta(t) = \frac{t}{\tau_\beta} \exp\left(-\frac{t}{\tau_\beta}\right). \tag{2.12}$$

Note that $G^{syn}_{ij\alpha\beta}$ has the dimension of a current density and that excitatory (resp. inhibitory) interactions correspond to $G^{syn}_{ij\alpha\beta} > 0$ (resp. $G^{syn}_{ij\alpha\beta} < 0$).

The synaptic current, which a cell i of the αth population receives from a cell j from the βth population, is

$$I^{syn}_{i\alpha\beta}(t) = \sum_j I^{syn}_{ij\alpha\beta}(t), \tag{2.13}$$

where $\alpha = E, I$, $i = 1, \ldots, N_\alpha$, $j = 1, \ldots, N_\beta$, and N_α is the number of neurons in the αth population. As a limiting case of a network with extensive connectivity, we assume full connectivity between the neurons, which simplifies considerably our analytical approach. For simplicity, we also assume that the strength of a synapse between two neurons depends on only the populations to which they belong. Therefore,

$$G^{syn}_{ij\alpha\beta} = G^{syn}_{\alpha\beta}\,. \tag{2.14}$$

In the case of an extensively connected network, the average number of synaptic inputs per neuron varies proportionally to the size of the system, and the synaptic strengths are varied in inverse proportion to the system size so that (see Hansel & Sompolinsky, 1996)

$$G^{syn}_{\alpha\beta} = \frac{g_{\alpha\beta}}{N_\beta}, \tag{2.15}$$

where the normalized synaptic strengths, $g_{\alpha\beta}$ are independent of the N_α's. Our approach can be applied to the case where the kinetics of excitatory (resp. inhibitory) synapses are different when the postsynaptic neuron belongs to the excitatory or the inhibitory population. However, this entails

an increase in the number of parameters of the model. Therefore, in this article, we consider that the synaptic rise time and decay time depend on only the nature, excitatory or inhibitory, of the synapses, and not on the synapse target. The rise and decay times of the synapses are denoted by $\tau_{1\beta}$, $\tau_{2\beta}$, $\beta = E, I$. We neglect axonal propagation delays.

3 The Asynchronous State and Its Stability

3.1 The Distribution of Neuron Firing Rates in the Asynchronous State. In the asynchronous state, the synaptic current is the same for all neurons in a population and does not depend on time. It is given by

$$I_{i\alpha}^{syn}(t) = \sum_{\beta=E,I} g_{\alpha\beta}\nu_\beta \equiv I_\alpha^{syn}, \tag{3.1}$$

where ν_β is the average firing rate of the neurons in population β and $g_{\alpha\beta}$ is a 2×2 matrix that characterizes the strengths of the synaptic interactions within and between the populations. Integrating the dynamical equations, equation 2.7, one calculates the firing rate of each of the neurons in the network. This yields

$$\begin{aligned}\nu_{i\alpha} &= \left[\int_{V_r}^{V_t} \frac{dV}{V^2 + I_{i\alpha} + I_\alpha^{syn} - I_\alpha^{th}}\right]^{-1} \\ &\equiv F\left(I_{i\alpha} + \sum_{\beta=E,I} g_{\alpha\beta}\nu_\beta - I_\alpha^{th}\right),\end{aligned} \tag{3.2}$$

where

$$F(I) = \frac{\sqrt{I}}{\arctan(V_t/\sqrt{I}) - \arctan(V_r/\sqrt{I})} \tag{3.3}$$

if $I > 0$ and $F(I) = 0$ otherwise. These equations, together with

$$\nu_\alpha = \frac{1}{N_\alpha}\sum_i \nu_{i\alpha}, \tag{3.4}$$

determine the distribution of firing rates in each population. Note that neurons with an external current smaller than $I_\alpha^{\min} = I_\alpha^{th} - I_\alpha^{syn}$ are below threshold and cannot fire.

The distribution $P_\alpha(\nu)$ of the firing rates of the neurons in population α in the asynchronous state can be related to the distribution of external currents via the input-output relation,

$$P_\alpha(\nu) = Q_\alpha(F^{-1}(\nu))|F^{-1'}(\nu)| + \delta(\nu)\int_{-\infty}^{I_\alpha^{\min}} dI Q_\alpha(I), \tag{3.5}$$

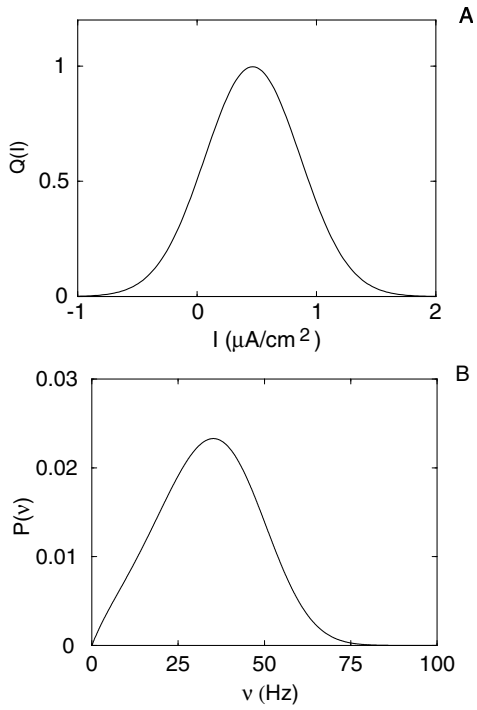

Figure 3: (A) Gaussian distribution of external current with a standard deviation $\sigma = 0.4$. (B) Distribution of firing rates for the QIF model (parameters as in Figure 1) and a distribution of currents as in A. The average firing rate is $\bar{\nu} = 30$ Hz. The delta function at $\nu = 0$ is not shown.

where the last contribution comes from the neurons that receive a total input too small to make them fire. The distribution of firing rates is plotted in Figure 3 for a gaussian distribution of currents:

$$Q_\alpha(I) = \frac{1}{\sqrt{2\pi\sigma_\alpha^2}} \exp\left(-\frac{(I - I_\alpha)^2}{2\sigma_\alpha^2}\right). \tag{3.6}$$

We emphasize that the distribution of firing rates can be kept constant even if the coupling strengths change. This can be done simply by adjusting the distribution of external currents with an offset that depends on the coupling and the average firing rate of the population. In this way, one can separate the effect of coupling strength and the effect of the average rate on synchronization properties.

3.2 Stability Analysis of the Asynchronous State. The stability of the AS in a homogeneous network of leaky integrate-and-fire neurons has been studied by Abbott and van Vreeswijk (1993). We have generalized their approach to the case of heterogeneous network of QIF neurons (Hansel & Mato, 2001).

For each of the active neurons in the population α, the variable $y_{i\alpha}$ can be defined as

$$y_{i\alpha} = \nu_{i\alpha} \int_{V_r}^{V_{i\alpha}} \frac{dx}{x^2 + I_{i\alpha} + \sum_\beta g_{\alpha\beta}\nu_\beta}, \tag{3.7}$$

where ν_i and ν_α are the firing rates of neuron i and the average population firing rate in the AS, respectively, and $g_{\alpha\beta}$ are the strengths of the synapses from population β to population α. This dynamical variable evolves in time according to

$$\frac{dy_{i\alpha}}{dt} = \nu_{i\alpha} + \sum_\beta g_{\alpha\beta} K_\beta(y_{i\alpha})\epsilon_\beta(t), \tag{3.8}$$

where

$$\epsilon_\beta(t) = \frac{1}{N_\beta} \sum_{j=1}^{N_\beta} (\nu_{j\beta}(t) - \nu_\beta) \tag{3.9}$$

is the deviation of the firing rate of neuron j at time t from its value in the AS, and

$$K_\alpha(y_{i\alpha}) = \frac{\nu_{i\alpha}}{V_{i\alpha}^2 + I_i + \sum_\beta g_{\alpha\beta}\nu_\beta}. \tag{3.10}$$

The probability density, $\rho_\alpha(y, \nu, t)$ satisfies the continuity equation,

$$\frac{\partial \rho_\alpha(y, \nu, t)}{\partial t} = -\frac{\partial J_\alpha(y, \nu, t)}{\partial y}, \tag{3.11}$$

where the flux $J_\alpha(y, \nu, t)$ is

$$J_\alpha(y, \nu, t) = \left(\nu_\alpha + \sum_\beta g_{\alpha\beta} K_\beta(y)\epsilon_\beta(t)\right) \rho_\alpha(y, \nu, t). \tag{3.12}$$

In the asynchronous state, $J_\alpha(y, \nu, t) = \nu_\alpha$. The deviations from this value, $j_\alpha(y, \nu, t) = J_\alpha(y, \nu, t) - \nu_\alpha$, due to perturbations from the AS state satisfy

$$\frac{\partial j_\alpha(y, \nu, t)}{\partial t} = \sum_\beta g_{\alpha\beta} K_\beta(y) \frac{d\epsilon_\beta(t)}{dt} - \nu_\alpha \frac{\partial j_\alpha(y, \nu, t)}{\partial y}. \tag{3.13}$$

For synaptic interactions modeled with a difference of exponentials (see equations 2.11), it is straightforward to show that equation 3.13 is equivalent to

$$\frac{d\epsilon_\alpha(t)}{dt} = -\gamma_{1\alpha}\epsilon_\alpha(t) + h_\alpha(t) \tag{3.14}$$

$$\frac{dh_\alpha(t)}{dt} = -\gamma_{2\alpha}h_\alpha(t) + \gamma_{1\alpha}\gamma_{2\alpha}\sum_\nu j_\alpha(1,\nu,t), \tag{3.15}$$

where $\gamma_{k\alpha} = 1/\tau_{k\alpha}$ for $k = 1, 2$. The perturbation j_α has to be evaluated at $y = 1$ because this corresponds to the crossing of the threshold, $V = V_t$ (see equation 3.7).

The AS is stable if small perturbations from the AS eventually decay. Assuming that $j_\alpha(y,\nu,t), \epsilon_\alpha(t), h_\alpha(t)$ are proportional to $\exp(\lambda t)$ and integrating equation 3.13, one finds after a straightforward but tedious calculation that λ satisfies

$$\prod_{\alpha=E,I}\left[\frac{(\lambda+\gamma_{1\alpha})(\lambda+\gamma_{2\alpha}) - \gamma_{1\alpha}\gamma_{2\alpha}g_{\alpha\alpha}U_\alpha}{\gamma_{1\alpha}\gamma_{2\alpha}}\right] = g_{EI}g_{IE}U_IU_E, \tag{3.16}$$

where

$$U_\alpha(\lambda) = \int_0^\infty d\nu \frac{H_\alpha(\nu)}{1-\exp(-\lambda/\nu)} \tag{3.17}$$

and

$$H_\alpha(\nu) = \frac{P_\alpha(\nu)\nu}{2F^{-1}(\nu)}\left[1-\exp(-\lambda/\nu)\right.$$
$$\left. + \frac{(\cos(A+\phi)+\sin(A+\phi)\frac{A\nu}{\lambda}) - \exp(-\lambda/\nu)(\cos(\phi)+\sin(\phi)\frac{A\nu}{\lambda})}{1+(A\nu/\lambda)^2}\right] \tag{3.18}$$

with

$$A = 2\sqrt{F^{-1}(\nu)}/\nu \tag{3.19}$$

$$\phi = 2\arctan(V_r/\sqrt{F^{-1}(\nu)}). \tag{3.20}$$

The spectral equation, equation 3.16, determines the eigenvalues of the dynamical equations linearized around the AS. Note that this spectral equation also holds if a fraction of the neurons are subthreshold and do not fire in the AS. Indeed, an infinitesimal perturbation cannot make these neurons fire. Therefore, they do not contribute to the destabilization of the AS.

3.3 The Spectral Equation at the Onset of an Instability. The AS is stable if all the eigenvalues, the solutions to equation 3.16, have a negative real part. Therefore, continuous onset of instabilities occurs when at least one of the eigenvalues crosses the imaginary axis when some parameter is changed. At this onset, $\lambda = i\mu$ and singularities appear in the integral in equation 3.17. These singularities can be isolated, and one finds:

$$U_\alpha(i\mu) = \left(\frac{A_{1\alpha}}{2} + \frac{\pi}{\mu}A_{2\alpha} - i\frac{\mu}{2}A_{3\alpha}\right), \tag{3.21}$$

where

$$A_{1\alpha} = \int_0^\infty d\nu H_\alpha(\nu) \tag{3.22}$$

$$A_{2\alpha} = \sum_{n=1}^{\infty} H_\alpha\left(\frac{\mu}{2\pi n}\right)\left(\frac{\mu}{2\pi n}\right)^2 \tag{3.23}$$

$$A_{3\alpha} = \sum_{n=1}^{\infty}\int_{-\pi}^{\pi} dy \,\mathrm{ctg}\left(\frac{y}{2}\right)\frac{H_\alpha(\frac{\mu}{y+2n\pi})}{(y+2n\pi)^2} + \int_0^\pi dy \,\mathrm{ctg}\left(\frac{y}{2}\right)\frac{H_\alpha(\frac{\mu}{y})}{y^2}. \tag{3.24}$$

These integrals are nonsingular. In general, they have to be evaluated numerically. The onset of instabilities of the AS is determined by taking the real and imaginary part of equation 3.16. The simultaneous solution of these equations determines μ and the coupling at the onset of instabilities as a function of the other parameters of the model.

At instability onset, the synaptic currents in the unstable mode oscillate with a frequency given by the imaginary part of the eigenvalue, μ. The dephasing δ between the oscillations of the two populations is

$$\exp(i\delta) \propto \epsilon_I/\epsilon_E = \frac{g_{EE}U_E - (\lambda/\gamma_{1E}+1)(\lambda/\gamma_{2E}+1)}{|g_{EI}|U_I}. \tag{3.25}$$

A positive (resp. negative) value of the phase lag δ means that the oscillation of the inhibitory population is in advance (resp. delayed) over the excitatory population.

The solutions of equation 3.16 can be classified according to the temporal properties of the corresponding unstable modes of instability. If $\mu \neq 0$, the instability occurs through a Hopf bifurcation (Strogatz, 2000). This can happen in two ways. In the first, called a supercritical Hopf bifurcation, the AS loses stability, and simultaneously stable oscillations of the network activity appear with vanishingly small amplitude and finite frequency. The latter

is equal to $\mu/2\pi$. The phase lag between the inhibitory and the excitatory population activity is δ (see equation 3.25). In the second, called a subcritical Hopf bifurcation, the AS loses its stability by coalescing with an unstable state in which the activity of the network oscillates. This is a necessary (but not sufficient) condition for having a region in the parameter space where the stable AS coexists with two states of synchronous oscillations—one stable and one unstable. The stable oscillatory state persists in some regions where the AS is unstable and the unstable oscillatory state no longer exists. The values of μ and δ determined by the stability analysis now correspond to the frequency and the phase lag between the two populations in the unstable oscillatory state at bifurcation. However, if the amplitude of the stable oscillations at the bifurcation is small, these values should also provide a good estimate of the frequency and the phase lag in the stable oscillatory state near the bifurcation. This point needs to be verified with numerical simulations (see section 6). Finally, if $\mu = 0$, there is a saddle node (SN) bifurcation (Strogatz, 2000).

To study how the stability of the asynchronous states depends on the synaptic properties, we construct phase diagrams for a fixed distribution of the firing rates of the two populations, $P_E(\nu)$ and $P_I(\nu)$, taking as parameters the strength of the four interactions. This implies that when the interaction strengths are changed, the external average inputs (or the firing thresholds) have to be modified accordingly to satisfy equation 3.2 for the two populations. Because of the normalization of the synaptic interactions, changing the synaptic time constants does not affect the firing-rate distribution in the AS. To study their role on the emergence of synchrony, the synaptic time constants can be varied while maintaining constant all the other parameters.

4 Synchrony in a Two-Population Model: The Symmetric Case

A detailed analysis of the conditions of the AS stability as a function of synaptic coupling strength, synaptic kinetics, and distributions of firing rates is a formidable task. In this section, we focus on a situation where, $\tau_{1E} = \tau_{1I} = \tau_1$, $\tau_{2E} = \tau_{2I} = \tau_2$, and $P_E(\nu) = P_I(\nu)$. We term this situation the symmetric case. It turns out that to a large extent, this case can be investigated analytically and that the results thus obtained are highly instructive for understanding the general properties of the two-population network.

4.1 The Instabilities of the Asynchronous State. In the symmetric case, for all α, $U_\alpha(\lambda) = U(\lambda)$ where $U(\lambda)$ is given by equation 3.17. Therefore equation 3.16 becomes

$$(i\mu + \gamma_1)^2(i\mu+\gamma_2)^2 - \gamma_1\gamma_2(i\mu+\gamma_1)(i\mu+\gamma_2)U\mathcal{T} + \gamma_1^2\gamma_2^2U^2\mathcal{D} = 0, \qquad (4.1)$$

where U is a function of μ, $\mathcal{T} = g_{EE} + g_{II}$ and $\mathcal{D} = g_{EE}g_{II} - g_{EI}g_{IE}$. The latter parameters are the trace and the determinant of the matrix $g_{\alpha\beta}$, respectively.

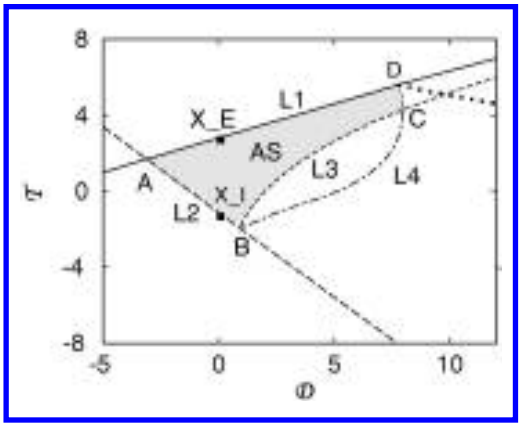

Figure 4: Phase diagram of a two-population QIF network in the symmetric case. The determinant and the trace of the coupling matrix are $\mathcal{D} = g_{EE}g_{II} - g_{EI}g_{IE}$ and $\mathcal{T} = g_{EE} + g_{II}$, respectively. The standard deviation of the current distribution is $\sigma_E = \sigma_I = 0.1$. The average firing rates in the AS are $\nu_E = \nu_I = 50$ Hz. The synaptic time constants are $\tau_{1E} = \tau_{1I} = 1$ msec, $\tau_{2E} = \tau_{2I} = 4$ msec. In the gray region, the AS is stable. See the text for an explanation of the different lines. The dotted line is the limit of L4 in the limit of infinite synaptic time constants (see section 5.3).

Therefore, one can completely describe the role of the synaptic strength in a two-dimensional plane spanned by these two effective parameters.

Let us consider point $X_0 = (\mathcal{D} = 0, \mathcal{T} = 0)$. A particular realization of point X_0 is obtained in the absence of coupling. Therefore, at X_0, the AS is marginally stable if the system is homogeneous, that is, for $\sigma_E = \sigma_I = \sigma = 0$. If one introduces any level of heterogeneities, the AS becomes stable in some region around this point. The size of this region depends on σ (or, equivalently, on the dispersion of the firing rates in the AS). This result holds independent of the parameters and the firing rates distribution provided the symmetry is preserved. It shows that there is always some domain in the $\mathcal{D}, \mathcal{T}$ plane where the AS is stable.

What are the boundaries of this region, and what are the instabilities on these boundaries? An example of the network phase diagram is shown in Figure 4. It was obtained by solving equation 4.1 for synaptic rise and decay times of 1 msec and 4 msec, respectively, the average firing rate of the two populations, $\nu = 50$ Hz, and the standard deviation of the external input distribution, $\sigma = 0.1$. The distribution of firing rates for these parameters is shown in Figure 3. The region of stability of the AS is bounded by four lines.

Line L1 is deduced from equation 4.1 by taking $\mu = 0$. It is straightforward to see that the equation of the line is given by

$$\mathcal{T} = U(0)\mathcal{D} + 1/U(0) \tag{4.2}$$

with

$$U(0) = \int_0^\infty d\nu \frac{P(\nu)\nu}{2F^{-1}(\nu)} \left[1 + \frac{\sin(A+\phi) - \sin(\phi)}{A}\right]. \tag{4.3}$$

For the parameters of Figure 4, $U(0) = 0.36$. On this line, an SN bifurcation occurs. Above the line, the AS with $\nu_E = \nu_I = 50$ Hz is unstable through an SN bifurcation. At the instability onset, the unstable mode grows exponentially but does not oscillate. This corresponds to a change in the average firing rates of the two populations, ν_E and ν_I, but not to the emergence of synchrony in the network.

Before discussing the general meaning of transition line L2, we consider two cases:

1. $P \equiv g_{EI}g_{IE} = 0, g_{II} = 0, g_{EE} > 0$. The two populations are noninteracting, and the inhibitory neurons are decoupled. For such parameters, the states of the network are represented in the $(\mathcal{D}, \mathcal{T})$ plane by the line segment: $\mathcal{D} = 0, \mathcal{T} > 0$. There is one instability with real eigenvalue for the unstable mode on this segment at point $X_E = (0, 1/U(0))$, which belongs to L1. All other instabilities in this segment occur in the region above L1 (not shown in Figure 4). Therefore, for the parameters of the figure, the excitatory population cannot develop synchrony by itself.

2. $P = g_{EI}g_{IE} = 0$, $g_{EE} = 0$, $g_{II} < 0$. As in the previous case, the two populations are noninteracting, but now the excitatory neurons, rather than the inhibitory ones, are decoupled. This situation is mapped in the phase diagram on segment $\mathcal{D} = 0, \mathcal{T} < 0$. An instability with a pure imaginary eigenvalue $\lambda = i\mu_c$ occurs on this segment at point $X_I = (0, g_c)$ where g_c and μ_c are solutions to the complex equation:

$$(i\mu_c + \gamma_1)(i\mu_c + \gamma_2) = \gamma_1\gamma_2 g_c U(i\mu_c). \tag{4.4}$$

Solving this equation yields $g_c = -0.98, \mu_c = 3.02$, that is, $\mu_c/(2\pi\nu_I) \approx 0.96$. Therefore, at X_I, the mutual inhibitory interactions I-I become strong enough to destabilize the AS with a Hopf bifurcation where synchrony emerges on the timescale of the spiking average period. Other solutions of equation 4.4 exist, but they are not relevant since they occur in the region below X_I, where the AS is already unstable. This mechanism, where synchrony of neural activity emerged in one population of neurons, has been studied by several authors

(van Vreeswijk,1996; Wang & Buszáki, 1996; White, Chow, Ritt, Soto-Treviño, & Kopell, 1998; Neltner, Hansel, Mato, & Meunier, 2000; Golomb & Hansel, 2000; Golomb, Hansel, & Mato, 2001).

We now consider the general case, $P = g_{EI}g_{IE} \neq 0$, in which the two populations interact.

It is straightforward to see that if $\mathcal{T}$ and $\mathcal{D}$ satisfy the relationship

$$\mathcal{T} = \frac{\mathcal{D}}{g_c} + g_c, \tag{4.5}$$

then equation 4.1 is satisfied with $\mu = \mu_c$.

Equation 4.5 defines a straight line (L2) in the $(\mathcal{T}, \mathcal{D})$ plane on which a Hopf bifurcation occurs. Obviously X_I belongs to this line. The intersection of L1 and L2 defines a point, $A \approx (-2.72, 1.8)$, where the real parts of the two eigenvalues vanish. One corresponds to an SN bifurcation and the other to a Hopf bifurcation. At that point, the AS becomes unstable through a codimension 2 bifurcation called a Gavrielov-Guckenheimer bifurcation (Kuznetsov, 1998). The points on L1 and L2 to the left of A are not relevant as instability onset since they are inside a region where the AS is already unstable.

The pattern of synchrony into which population α ($\alpha = E, I$) settles depends in general on the ratio

$$R_\alpha = \frac{\mu}{2\pi\nu_\alpha}. \tag{4.6}$$

Here R_α is close to one, and neurons fire on the average about one spike per period in the unstable mode. However, the phase relationship between the spikes and the collective oscillations can change from cycle to cycle. Consequently, the phase distribution is broad but unimodal.

It can be easily shown that on L2,

$$\frac{\epsilon_I}{\epsilon_E} = \frac{g_{EE} - g_c}{|g_{EI}|}. \tag{4.7}$$

Therefore, on this line, the phase lag is constant, $\delta = 0$, that is, at the instability onset, the activities in the two populations oscillate in phase.

Point B on L2 defined by $\mathcal{D} = g_c^2 \equiv \mathcal{D}_B$, $\mathcal{T} = 2g_c \equiv \mathcal{T}_B$ is a multicritical point where two eigenvalues have a vanishing real part. This can be shown by expanding equation 3.16 in the vicinity of B. One finds two other critical lines, L3 and L4, tangent to L2 in B. Sufficiently close to B, these lines are given by the equation

$$\mathcal{T} - \mathcal{T}_B = \beta_1(\mathcal{D} - \mathcal{D}_B) + \beta_2(\mathcal{D} - \mathcal{D}_B)^2, \tag{4.8}$$

where

$$\beta_1 = \frac{1}{g_c} \tag{4.9}$$

$$\beta_2 = -\frac{|W'(\mu_c)|^2}{4g_c^3 \Re e(W'(\mu_c))^2}. \tag{4.10}$$

Here we have defined $W(\mu) = \gamma_1\gamma_2 U(i\mu)/(i\mu + \gamma_1)(i\mu + \gamma_2)$, and $W'(\mu)$ is the derivative of W with respect to μ. For the parameters of Figure 4, $\beta_1 = -1.02$ and $\beta_2 = 47.9$. Hence, the expansion, equation 4.8, truncated at second order, is a good approximation to L3 and L4, only very close to B. This is why it seems to be a cusp in point B. Beyond B, L2 is no longer relevant for the instability of the AS.

We conclude that on AB, the AS undergoes an instability to spike-to-spike synchrony. This instability, driven by the I-I interactions, is the extension in the framework of two populations of the instability that occurs in one population of inhibitory neurons. The interaction between the two populations makes this mechanism less efficient. Indeed, from equation 4.5, one sees that when the feedback between the two populations increases, a stronger mutual inhibitory coupling, g_{II}, is required for the AS to be destabilized on L2.

Point D is defined as the intersection of L4 and L1. At that point, the AS is unstable through a codimension 2 bifurcation called a Takens-Bogdanov bifurcation (Kuznetsov, 1998). The coordinates of D can also be obtained by expanding equation 3.16 in the limit $\mu \to 0$. One finds that in D, $\mathcal{D} = U(0)^2$, $\mathcal{T} = 2U(0)$.

The frequency of the unstable mode, μ, varies continuously on L3 and L4, as shown in Figure 5. On L4, μ decreases continuously when $\mathcal{D}$ increases, from $\mu = \mu_{II}^c = 3.02$ at B, to $\mu = 0$ at D. On L3, μ increases slowly when $\mathcal{D}$ increases. In the limit of large $\mathcal{D}$, μ converges asymptotically to a finite value, μ_∞, and L3 is asymptotic to the straight line defined by $\mathcal{T} = \mathcal{D}/g_\infty + g_c$, where g_∞ and μ_∞ satisfy the equation

$$(i\mu_\infty + \gamma_1)(i\mu_\infty + \gamma_2) = \gamma_1\gamma_2 g_\infty U(i\mu_\infty). \tag{4.11}$$

Note that this equation is identical to the spectral equation describing the stability of the AS in one population of neurons. For the parameters of Figure 4, $\mu_\infty \approx 3.82$ and $g_\infty \approx 6.5$.

The ratio between the frequency of the unstable mode and the average firing rate of the neurons, $R \equiv R_E = R_I$ (see equation 4.6), is plotted in Figure 5. This ratio is larger than 1 on L3. This means that the unstable mode oscillates faster than the average frequency of the neurons. However R increases by less than 25% on L3. Therefore, the synchrony that emerges is on the timescale of the spikes. In contrast, on L4, R varies from $R \approx 1$ near B to $R = 0$ in the vicinity of D. This means that along L4, the pattern

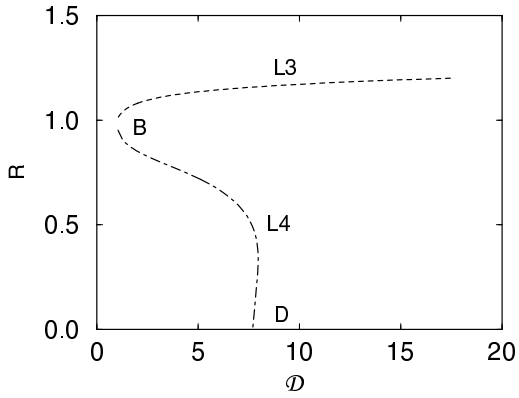

Figure 5: The ratio $R = \mu/2\pi\nu$ versus the determinant of the coupling matrix, $\mathcal{D}$, on lines L3 (dashed line) and L_4 (dashed-dotted line) shown in Figure 4. Points B and D correspond to B and D shown in Figure 4.

of synchrony changes continuously from spike-to-spike synchrony to burst synchrony in which the neurons have the time to fire several spikes on average during one period of oscillation of the unstable mode.

The phase lag, δ, on L3 and L4 can be expressed analytically as a function of $\mathcal{D}$, $\mathcal{T}$, and g_{EE}. From equation 4.1 one finds that

$$(i\mu + \gamma_1)(i\mu + \gamma_2) = \frac{\gamma_1\gamma_2 U(i\mu)}{2}(\mathcal{T} \pm \sqrt{\mathcal{T}^2 - 4\mathcal{D}}). \tag{4.12}$$

Analyzing the numerical solutions of the spectral equation, one finds that it is negative on L4 and positive on L3. Substitution in equation 3.25 gives for the phase lag the equation

$$\delta = \pm \arctan \frac{\Im_m(\sqrt{\mathcal{T}^2 - 4\mathcal{D}})}{g_{EE} - g_{II}}, \tag{4.13}$$

where the positive (resp. negative) sign is for the phase lag on L4 (resp. on L3).

The condition $\mathcal{T}^2 - 4\mathcal{D} = 0$ defines a line in the phase diagram to which B, D and the point $\mathcal{T} = \mathcal{D} = 0$ belong. Therefore, $\mathcal{T}^2 - 4\mathcal{D} < 0$ on L3, except in B and D where $\mathcal{T}^2 - 4\mathcal{D} = 0$ (see definition of points B and D). Since $g_{EE} - g_{II} > 0$,

$$\cos\delta > 0. \tag{4.14}$$

The phase lag, δ, is a function of the three variables g_{EE}, g_{II}, and $g_{EI}g_{IE}$ and not only the reduced variables $\mathcal{T}$ and $\mathcal{D}$. In contrast to what happens on L2,

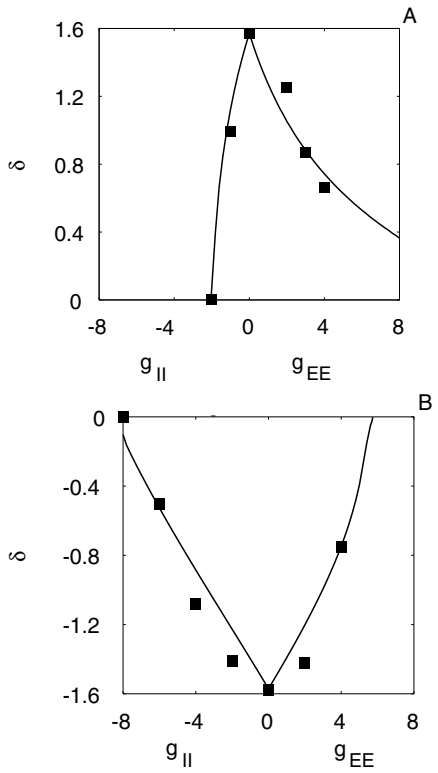

Figure 6: Phase lag of the population oscillations. Solid lines were obtained from equation 3.25. The squares are results from numerical simulations of a two-population network with $N_E = N_I = 1600$. The positive (resp. negative) part of the x-axis corresponds to variation of g_{EE} with $g_{II} = 0$ (resp. g_{II} with $g_{EE} = 0$). (A) In the vicinity of L3. The simulations were done keeping a fixed distance equal to 1 from L3 and with $g_{IE} = -g_{EI}$. The positive (resp. negative) part of the x-axis corresponds to variation of g_{EE} (resp. g_{II}). The standard deviation of the current distribution is $\sigma = 0.1$. Other parameters are as in Figure 4. (B) In the vicinity of L4. The simulations were done keeping a fixed distance equal to 2 from L4 and with $g_{IE} = -g_{EI}$. The standard deviation of the current distribution is $\sigma = 0.4$. Other parameters are as in Figure 4.

on L3 and L4, it changes continuously and nonmonotonically. It vanishes in B and D. This is shown, for example, in Figure 6A, where δ is plotted against g_{EE} (with $g_{II} = 0$) along the two-line segment L3 and L4 and against g_{II} (with $g_{EE} = 0$) for the same two lines.

Equation 4.14 implies that in general, $|\delta| < \pi/2$. In particular, the activity of the two populations can never be in antiphase. From equation 4.13, one

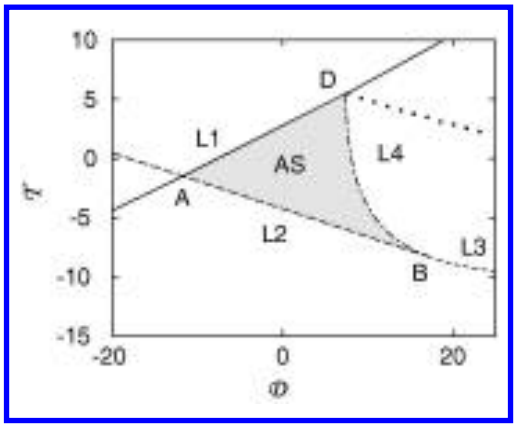

Figure 7: Phase diagram of a two-population QIF network in the symmetric case. The determinant and the trace of the coupling matrix are $\mathcal{D} = g_{EE}g_{II} - g_{EI}g_{IE}$ and $\mathcal{T} = g_{EE} + g_{II}$, respectively. The standard deviation of the current distribution is $\sigma_E = \sigma_I = 0.4$. Other parameters are as in Figure 4. In the gray region, the AS is stable. See the text for an explanation of the different lines. The dotted line is the limit of L4 for very large synaptic time constants (see section 5.3).

sees that the maximum phase lag at the onset of instability, $|\delta| = \pi/2$, is achieved only for $g_{EE} = g_{II} = 0$ ($\delta = -\pi/2$ on L3 and $\delta = \pi/2$ on L4). Finally, on line L3, in the limit of very large $\mathcal{D}$ and $\mathcal{T}$, the phase lag returns to 0, as can be seen in equation 3.25 using equation 4.11. These results are also confirmed in the example of Figure 6B.

The two line segments, L3 and L4, intersect at point C where $\mathcal{D}(C) \approx 7.9$ and $\mathcal{T}(C) \approx 4.3$. Note that μ has different values on the two lines at C, as can be seen from Figure 5. Therefore, at C, the AS is unstable through a double-Hopf bifurcation (Kuznetsov, 1998). Whether L3 or L4 is the border of stability of the AS depends on $\mathcal{T}$. This is shown in Figure 4 for $\mathcal{T} > \mathcal{T}(C)$. The AS loses stability on L4, whereas for $\mathcal{T} < \mathcal{T}(C)$, this occurs on L3.

4.2 The Effect of Heterogeneities. We now consider how the phase diagram for the stability of the AS is modified when the level of heterogeneities varies.

Figure 7 shows the phase diagram in the symmetric case for $\sigma_E = \sigma_I = 0.4$, with all other parameters the same as in Figure 4. Comparing these two figures, one sees that in spite of a significant increase in the level of heterogeneities, the transition line (L1) has moved only slightly. In contrast, L2 has substantially moved toward more negative values of $\mathcal{T}$ and $\mathcal{D}$. This can be easily understood because to compensate for the increased desynchronizing effect of the heterogeneities, stronger synapses are required to destabilize the AS. Line segment L4 is barely modified in the neighborhood of D, its crossing point with L1. A stronger effect occurs in the vicinity of

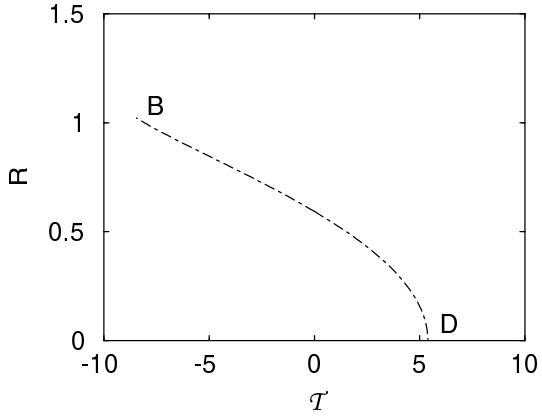

Figure 8: The ratio $R = \mu/2\pi\nu$ versus the trace of the coupling matrix, $\mathcal{T}$, on line L_4 shown in Figure 7. Points B and D correspond to B and D shown in Figure 7.

B, which moves this point toward more negative values of $\mathcal{T}$ and $\mathcal{D}$. Most of the changes in line segment L4 when σ increases can be explained by this stronger effect. A more dramatic change occurs for the line segment L3. Indeed, when the heterogeneities are strong enough, L3 moves completely to the right of L4. Moreover, on L4, $\mathcal{T}$ increases very slowly with $\mathcal{D}$. Therefore, all L3 becomes located well into the region where the AS is already unstable, and this instability scenario is now irrelevant.

As in Figure 4, along line L4, the frequency of the unstable mode depends continuously on the location. However, in contrast to that case, L4 is relevant as an instability line all the way between points B and C. In Figure 8, we plotted the ratio of the frequency of the emerging oscillations to the average firing rate showing the continuous and monotonic variation of this quantity along L4 from a value slightly larger than 1 at B corresponding to spike-to-spike synchrony to 0 at D in the vicinity of which the network fires in synchronous bursts.

To characterize further how the instabilities of the AS depend on the level of heterogeneities, we computed the value of $\mathcal{D}$ on the four lines L1, L2, L3, L4 as functions of the heterogeneity level, σ, for $\mathcal{T}$ with all other parameters constant. The results are shown in Figure 9. As already noted from the comparison of Figures 4 and 7, the location of L1 depends only very weakly on the level of the heterogeneities. In contrast, the destabilization of line L2 is much more sensitive to this parameter. In Figure 9B, the line segment L3 is clearly much more sensitive to heterogeneities than line segment L4. Indeed, the coupling strength required on the former line increases much more rapidly with σ than on the latter line. A consequence of this difference in sensitivity to heterogeneities is that, as already noted, the two line segments

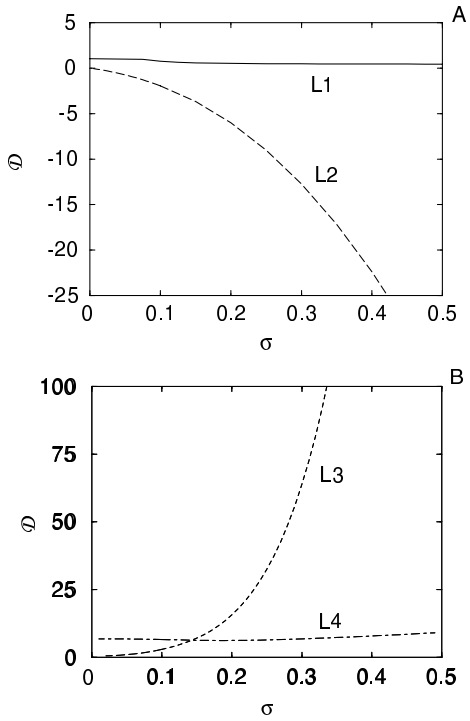

Figure 9: Determinant of the coupling matrix, $\mathcal{D}$, versus the standard deviation, σ on the bifurcation lines L1, L2, L3, L4 for $\mathcal{T} = 1$. The synaptic time constants are as in Figure 4. (A) L1 (solid line) and L2 (long dashed line). (B) L3 (dashed line) and L4 (dashed-dotted line).

L3 and L4 interchange their positions in the ($\mathcal{D}$,$\mathcal{T}$) phase diagram when σ is large enough. This happens at $\sigma \approx 0.15$. For σ larger than this value, line L3 is located beyond the instability line L4 in a region where the AS is already unstable. Therefore, in that case only, one instability scenario driven by the E-I-E interaction loop is relevant.

4.3 The Effect of the Firing Rate. For a fixed architecture and coupling strength, the average firing rate of the network depends on the external input. To investigate how the stability of the AS depends on this input, we studied the solutions of the spectral equation as a function of the average firing rate, keeping the variance of the threshold distribution constant, $\sigma = 0.1$.

Figure 10A shows how the minimal coupling strength g_c required for the destabilization of the AS in one inhibitory population determined by equa-

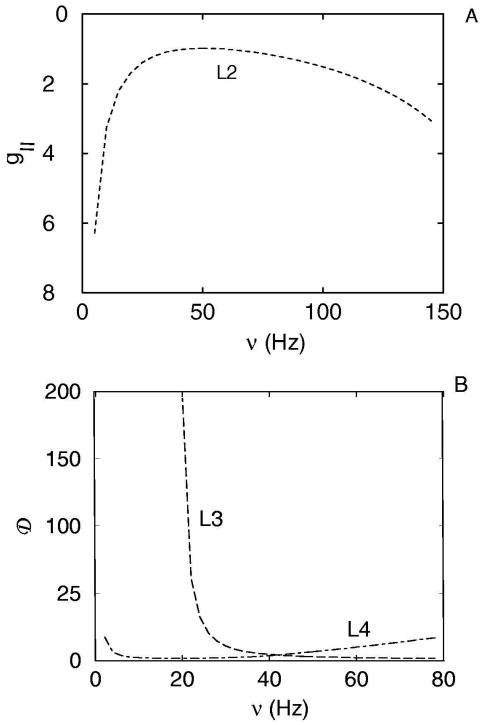

Figure 10: (A) The synaptic coupling, g_{II}, at which the AS becomes unstable in one inhibitory population versus the average firing rate of the neurons. The standard deviation of the input distribution is $\sigma = 0.1$. The synaptic time constants are as in Figure 4. (B) The determinant, $\mathcal{D}$, on the bifurcation lines L3 (dashed line) and L4 (dashed-dotted line) versus the average firing rate of the neurons in a two-population network (symmetric case) for $\mathcal{T} = 1$. Other parameters are as in Figure 4.

tion 4.4 varies with the average firing rate. One finds that g_c is a nonmonotonic function of the average firing rate. The critical coupling is minimum ($g_c = -0.98$) for a firing rate of $\nu = 50$ spikes per second. Note, however, that the extremum of the curve is very shallow. Already for $g_c = -1.5$, the AS is unstable in a broad range of average firing rates.

Figure 10B plots $\mathcal{D}_c$, the value of $\mathcal{D}$ at the instability onset on L3, and L4, for $\mathcal{T} = 1$. This figure shows that on L3, $\mathcal{D}_c$ decreases monotonically with increasing firing rate. Moreover, this instability disappears for $\nu < \nu_{\min} = 20$ spikes per second at which value $\mathcal{D}_c$ diverges. In contrast, on L4, $\mathcal{D}_c$ is a nonmonotonic function of the average firing rate and exists at all values of the firing rate. The two lines intersect for $\nu \approx 40$ spikes per second. Below

this value of the firing rate, the relevant instability of the AS is on L3, whereas above this value, it is on L4.

4.4 Summary of the Results in the Symmetric Case. Our analysis of the symmetric case reveals that in a two-population heterogeneous network, the AS can lose stability in four ways. Two of these are not specific to two-population networks and are an extension in this framework of instabilities that already exist for one population: the rate instability that occurs on L1 and the spike-to-spike synchrony instability that occurs on L2. At the onset of the former type of instability, which depends only weakly on heterogeneities, no synchrony occurs. In the latter case, which is sensitive to heterogeneities, at the onset of the instability, activities in the two populations are synchronized on the timescale of the spikes and oscillate in phase. The two other types of instability that occur on L3 and L4 are specific to two-population networks. On L3, the activities in the two populations oscillate at a frequency on the order of the average firing rate, and the inhibitory population is oscillating ahead of the excitatory population. On L4, the frequency of the population activity oscillations can become very slow. This happens if both the recurrent excitation and the recurrent inhibition (the feedback between the two populations) are strong. On L4, the oscillation of the excitatory population is ahead of the oscillation of the inhibitory population. Finally, L3 and L4 differ in the way they depend on the level of heterogeneities. L3 becomes irrelevant if the heterogeneities are large or the average firing rates are small.

5 Synchrony in Two-Population Networks: The General Case

If the distributions of the firing rates of the two populations are different in the AS or the synaptic time constants of the excitation and inhibition are not the same, the stability of the AS (at given firing-rate distributions) depends on three synaptic coupling parameters g_{EE}, g_{II}, $g_{EI}g_{IE}$ and also on the synaptic time constants.

5.1 The Effect of the Synaptic Coupling Strength. Figure 11A displays the phase diagram of the AS in the plane $-g_{EI}g_{IE}$, g_{EE} when $g_{II} = 0$. The synaptic time constants are $\tau_{1E} = 1$ msec, $\tau_{2E} = 3$ msec, $\tau_{1I} = 1$ msec, and $\tau_{2I} = 6$ msec. The average firing rate of the excitatory (resp. inhibitory) population is 20 Hz (resp. 40 Hz), and $\sigma_E = \sigma_I = 0.2$ for both populations. As in the symmetric case, if the recurrent excitation is strong enough, SN instability occurs. In the plane $-g_{EI}g_{IE}$, g_{EE}, this instability occurs on a straight line, the equation of which is

$$g_{EE} = \frac{1}{U_E(0)} - g_{EI}g_{IE}U_I(0), \tag{5.1}$$

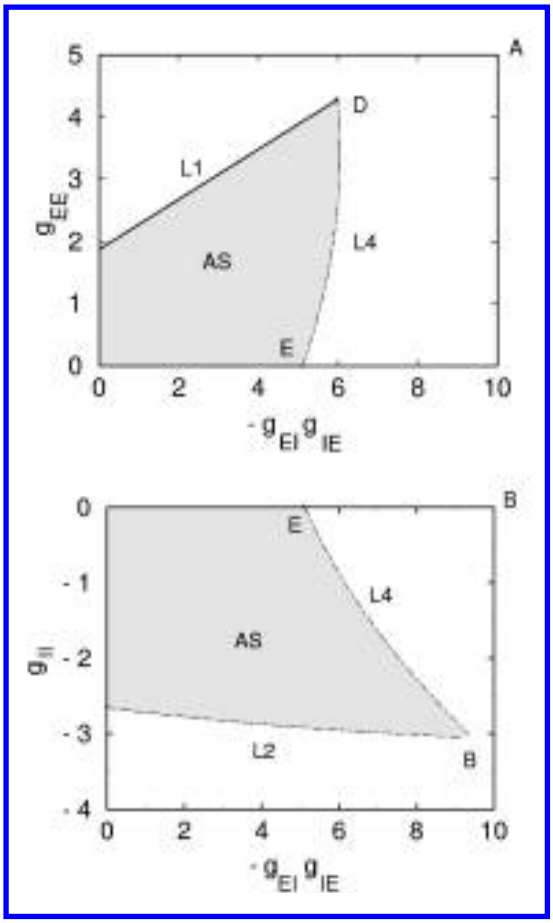

Figure 11: Phase diagram in the asymmetric case. The average firing rate of the excitatory (resp. inhibitory) population is $\nu_E = 20$ Hz (resp. $\nu_I = 40$ Hz). The synaptic time constants are $\tau_{1E} = \tau_{1I} = 1$ msec, $\tau_{2E} = 3$ msec, $\tau_{2I} = 6$ msec. The standard deviations of the input distributions are $\sigma_E = \sigma_I = 0.2$. The AS is stable in the gray region. In this figure, only the physical branches of the instability lines are drawn. In particular, L3, which branches at B, is not drawn. (A) $g_{II} = 0$. A saddle-node bifurcation occurs on L1 (solid line) and a Hopf bifurcation on L4 (dashed-dotted line). (B) $g_{EE} = 0$. Hopf bifurcations occur on L2 (long-dashed line) and L4 (dashed-dotted line). The difference between these two bifurcation lines is explained in the text. At E, the instability of the AS is due to the interactions between the two populations since $g_{EE} = g_{II} = 0$ at that point.

where $U_\alpha(0), \alpha = E, I$ is given by equation 4.3, replacing the distribution P by P_α, the firing-rate distribution in population α. For the parameters of the figure, one finds $U_E(0) = 0.53$ and $U_I(0) = 0.4$. When g_{EE} increases, this instability can be prevented by increasing the negative feedback between the two populations measured by $g_{EI}g_{IE} < 0$. When this feedback is strong enough, the AS becomes unstable through a Hopf bifurcation, which occurs on the line to the right of the phase diagram. On this line, the period of the population rhythm varies continuously from $\mu \approx 1.25$ at its intersection with the x-axis, E, ($g_{EE}(E) = 0$) to $\mu = 0$ at D. The value of μ at E corresponds to a pattern in which the inhibitory (resp. excitatory) neurons fire approximately two spikes (resp. one spike) per period of the population oscillation. Near D, it corresponds to a pattern in which neurons tend to fire synchronous bursts with many spikes. The properties of the instability on this line are similar to those found on line L4 in the phase diagrams of the symmetric case. Because of these similarities, we have denoted this line by L4 here as well.

Figure 11B displays the phase diagram of the model in the plane $-g_{EI}g_{IE}$, g_{II} when $g_{EE} = 0$. The other parameters are the same as in Figure 11A. The region of stability of the AS is bounded by two lines. One, L2, corresponds to the destabilization of the AS when g_{II} is strong enough. Like line L2 in Figures 4 and 7, this line corresponds to the emergence of synchrony through the I-I interaction. In contrast to the symmetric case, here $\mu/2\pi$ and δ are not constant on L2. However, $\mu/2\pi$ always remains just slightly smaller, by less than 4%, than the average firing rate of the inhibitory population, and δ is always smaller than 15% of the total period.

Another difference with the symmetric case is that L2 is not straight anymore. However, it deviates only slightly from a straight line. In similarity with the symmetric case, the slope of L2 is negative. This means that the feedback between the two populations plays against synchrony through the I-I coupling. A stronger I-I coupling is required to compensate for this feedback.

For strong enough feedback, $g_{EI}g_{IE}$, the AS can lose stability even if g_{II} is small. This transition occurs on the line to the right in Figure 11B. On this line, the population frequency varies significantly. Indeed, at B, $\mu/2\pi \approx 40$ Hz, and it is two times smaller at point E. Embedded into the three-dimensional space, (g_{EE}, g_{II}, $g_{EI}g_{IE}$), this line connects to L4 from Figure 11A. We also denote this line by L4 since the instabilities occurring on these two lines can be thought of as corresponding to a similar synchrony mechanism. Note that the slope of L4 in Figure 11B is negative. In other words, increasing g_{II} plays against the destabilization of the AS through this mechanism.

5.2 The Effect of Synaptic Time Constants. In this section, we analyze the effect of synaptic kinetics on the stability of the AS for fixed distributions of firing rates. First, we focus on the effect of the decay times.

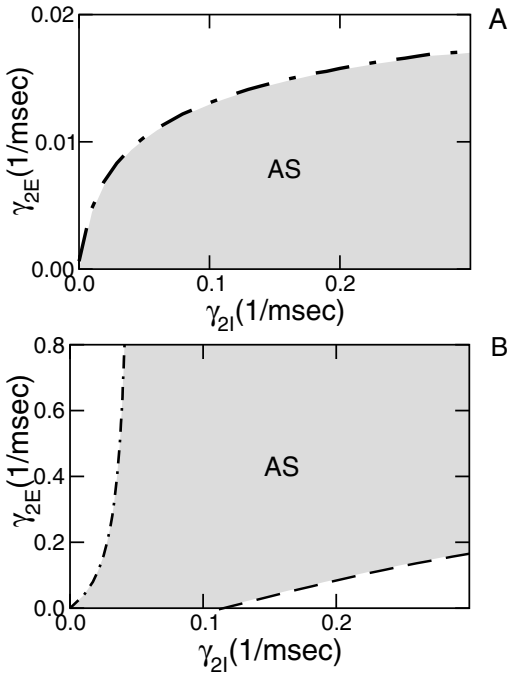

Figure 12: Phase diagrams in the plane $\gamma_{2I} \equiv 1/\tau_{2I}$, $\gamma_{2E} \equiv 1/\tau_{2I}$ for two different strengths of the I-I interactions. The average firing rate of the excitatory and inhibitory populations are $\nu_E = 20$ Hz and $\nu_I = 30$ Hz, respectively. (A) $g_{II} = 0$. (B) $g_{II} = -7.4$, Other parameters are $\tau_{1E} = \tau_{1I} = 1$ msec, $g_{EE} = 6$, $g_{EI}g_{IE} = -36$ and $\sigma_E = \sigma_I = 0.2$. In the gray region, the AS is stable. On L2 (long-dashed line) and L4 (dashed-dotted line), Hopf bifurcations occur. Along L4, the frequency of the unstable mode μ decreases with γ_{2I}. For instance, in A, $\mu/2\pi$ varies from 11 Hz for $\gamma_{2I} = 0.3$ msec^{-1} to 0 for $\gamma_{2I} = 0$. Along L2, μ remains finite and, its variation is smaller.

Figure 12 displays the phase diagram in the (γ_{2I},γ_{2E}) plane for $g_{EE} = 6$, $g_{EI}g_{IE} = -36$ and two different values of g_{II}. We consider first the case where $g_{II} = 0$. In the limit $\tau_{2E} \to \infty$, the AS is always stable. This is because in that limit, the excitatory input to the inhibitory population is not modulated in time. Therefore, it is equivalent to a positive constant current that excites the inhibitory population. The only way synchrony can occur in this case is through the I-I interactions, which we have assumed to be zero. For finite τ_{2E}, the AS is unstable provided τ_{2I} is sufficiently large. This defines a transition line $\gamma_{2E} = f(\gamma_{2I})$ where function $f(\gamma)$ is an increasing function that vanishes linearly when $\gamma \to 0$. On this line, which is plotted in Figure 12A, μ is a decreasing continuous

function of γ_{2I}. It goes to 0 in the limit $\gamma_{2I} \to 0$. Since the decay of the inhibition cannot be faster than its rise time (see equation 2.11), μ cannot be larger than $\mu = 0.79$, its value for $\tau_{2I} = 1$ msec, on the transition line in Figure 12A. Therefore, all along the line, the transition leads to a synchronous bursting state. The bursts are short for fast inhibition and long when the inhibition is slow. In Figure 12A, the AS stabilizes for fast inhibition and slow enough excitation. In particular, the fastest excitation compatible with a stable AS (attained for very fast inhibition with $\tau_{1I} = \tau_{2I} = 1$ msec) is $\tau_{2E} \approx 50$ msec, in the range of NMDA synaptic time constants.

The phase diagram in the (γ_{2I},γ_{2E}) plane remains qualitatively the same as in Figure 12A, provided that g_{II} is sufficiently small. If g_{II} is large enough, a second instability line appears in the region of the phase diagram corresponding to fast inhibition and slow excitation. This is because for a large enough g_{II}, the I-I interaction can induce spike-to-spike synchrony in the inhibitory population. This situation is shown in Figure 12B. Note that the transition line found for $g_{II} = 0$ (see Figure 12A) is still present but has been shifted to much higher values of γ_{2E}.

In contrast to what happens for small values of g_{II}, when the inhibition is fast ($\tau_{2I} < 9$ msec), the AS is destabilized for slow enough excitation. For instance, for $\tau_{2I} = 6$ msec, this happens for τ_{2E} larger than 20 msec. Note that for the parameters of Figure 12B, the AS is stable if the excitatory and inhibitory synapses are in a range corresponding to AMPA and $GABA_A$ synapses, respectively.

5.3 The Limit of Slow Synapses. The spectral equation, equation 3.16, can be simplified if one assumes that the synapses have infinitely long decay time constants. We assume that $\gamma_{2E} = \eta\bar{\gamma}_{2E}$ and $\gamma_{2I} = \eta\bar{\gamma}_{2I}$ where $\eta \ll 1$ and $\bar{\gamma}_{2E}$, $\bar{\gamma}_{2I}$ are finite and we make the ansatz

$$\lambda = \eta\bar{\lambda}. \tag{5.2}$$

Substituting in equation 3.16, expanding at the leading order in η, and using the fact that $\int_0^1 dy K(y) = F'(F^{-1}(\nu))$, one finds that at the onset of an instability $\bar{\lambda} = i\bar{\mu}$ with $\bar{\mu}$ solution of the equation,

$$((i\bar{\mu} + \bar{\gamma}_{2E}) - \bar{\gamma}_{2E} g_{EE} U_E)((i\bar{\mu} + \bar{\gamma}_{2I}) - \bar{\gamma}_{2I} g_{II} U_I) = g_{EI} g_{IE} \bar{\gamma}_{2E} \bar{\gamma}_{2I} U_E U_I, \tag{5.3}$$

where the quantities

$$\bar{U}_\alpha = \int_0^\infty d\nu P_\alpha(\nu) F'(F^{-1}(\nu)) \tag{5.4}$$

do not depend on $\bar{\mu}$.

Equation 5.3 is quadratic in $\bar{\mu}$. For $\bar{\mu} = 0$, one recovers the condition for the SN bifurcation obtained above (line L1). Another transition line is found for $\bar{\mu} \neq 0$ on which synchronous oscillations emerge and have a low frequency, $\mu \propto \eta \ll 1$. During one period of these oscillations, the neurons burst synchronously since they have the time to fire several spikes in one oscillation of the populations. If one assumes $\gamma_{2E} = \gamma_{2I} = \gamma$, it is convenient to define $X = g_{EE}U_E + g_{II}U_I$ and $Y = \mathcal{D}U_IU_E$. One finds that an instability to oscillations occurs on the line $X = 2$ in the (X, Y) plane and that $\mu \propto \eta \ll 1$ varies continuously on this line. Therefore, sufficiently strong g_{EE} and not too large g_{II} are required for burst synchrony. More generally, when $\gamma_{2E} \neq \gamma_{2I}$, this onset of slow bursting occurs on a surface in the three-dimensional space $(g_{EE}, g_{II}, -g_{EI}g_{IE})$. One also finds here that a sufficiently strong g_{EE} is required for this instability. In general, one also finds that increasing g_{II} prevents the emergence of synchronous bursting.

Equation 5.3 is also the spectral equation for the stability of the fixed-point solutions of the system of two coupled equations,

$$\frac{1}{\bar{\gamma}_{2E}}\frac{dv_E}{dt} = -v_E + G_E(g_{EE}v_E + g_{EI}v_I) \tag{5.5}$$

$$\frac{1}{\bar{\gamma}_{2I}}\frac{dv_I}{dt} = -v_I + G_I(g_{IE}v_E + g_{II}v_I), \tag{5.6}$$

where the functions $G_\alpha(h_E, h_I)$ are

$$G_\alpha(x) = \int_{-\infty}^{\infty} dI Q_\alpha(I) F(I + x). \tag{5.7}$$

Let us consider a two-population rate model in which the neurons have an input-output transfer function $F(x)$ and receive a random external input with probability density function $Q_\alpha(I)$ ($\alpha = E, I$). In this model, the firing rate of neuron i in population α, $v_{i\alpha}$, follows the equation

$$\frac{1}{\bar{\gamma}_{2\alpha}}\frac{dv_{i\alpha}}{dt} = -v_{i\alpha} + F(I_{i\alpha} + I_{i\alpha}^{syn}), \tag{5.8}$$

where the total synaptic current, $I_{i\alpha}^{syn}$, is given by equation 3.1 and $I_{i\alpha}$ is its external input. It is easy to check that the dynamics of this model can be reduced to two effective degrees of freedom: the average firing rate in the two populations, $v_\alpha(t), \alpha = E, I$, which satisfy equations 5.5 and 5.6. These two equations are nothing other than a two-population mean-field model with transfer function $G_\alpha(x)$ given by equation 5.7. An example of such a function is plotted in Figure 13. Therefore, in the limit of very slow synaptic decay, the instabilities of our spiking model are the same as those of a rate model (see also Ermentrout, 1994; Bressloff & Coombes, 2000).

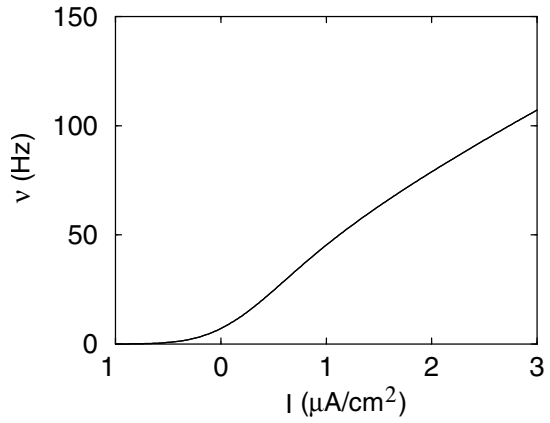

Figure 13: Input-output transfer function of the rate model that corresponds to the QIF model for $\sigma = 0.4$. Other parameters as in Figure 1.

Finally, one can show that if the rise time of the synapses is also very slow and on the same order of magnitude as their decay time, the quadratic equation for μ, equation 5.5, is replaced by a quartic equation. This situation is similar to the previous one except that now the instability to burst synchrony does not require mutual interactions between the excitatory neurons. Here too the spectral equation can be derived from the mean-field equations of a rate model. However, now it is defined by four coupled equations—two equations for each of the two populations.

5.4 The Effect of the Average Firing Rates. The effect of the firing rates of the two populations on the stability of the AS has been studied above in the symmetric case in which the average firing rates of the two populations were necessarily equal. Here, we consider the case in which the distributions of firing rates in the two populations are different to understand how this affects the stability of the AS. In particular, we want to investigate whether some specific relationship ("resonance") between the average firing rates in the two populations is favorable to the emergence of synchrony in the network.

The SN instability ($\mu = 0$) depends on the firing rates through $U_E(0)$ and $U_I(0)$. The maximal value of the recurrent excitatory feedback, g_{EE}, is given by

$$g_{EE} = \frac{1}{U_E(0)} + |g_{EI}|g_{IE}\frac{U_I(0)}{1+|g_{II}|U_I(0)}. \tag{5.9}$$

The quantities $U_\alpha(0)$, $\alpha = E, I$ are decreasing functions of the firing rate. For large firing rates, they converge to a finite value. Therefore, increasing

the firing rate of the excitatory population or decreasing the firing rate of the inhibitory population increases g_{EE} (i.e., stabilizes the AS with respect to the SN instability). In particular, the maximal value of g_{EE} at this onset of instability, when ν_I changes, is $1/U_E(0) + |g_{EI}|g_{IE}/g_{II}$. It is reached in the limit of very small firing rates of the inhibitory neurons. This is because the sensitivity of the neurons to changes in their input increases when their firing rate decreases. Therefore, the inhibitory neurons are more efficient at low firing rates than at high firing rates at preventing the runaway of the activity of the excitatory neurons due to the excitatory feedback.

In the symmetric case, we have found that the interaction with an excitatory population stabilizes the AS with respect to the spike-to-spike instability generated by the I-I interactions. Figure 11B provides an example that this remains true for the general case. In order to gain more insight into this property, we computed the value of g_{II} on L2 for different values of ν_E and ν_I with all the other parameters of the model held constant. The result for $\nu_I = 50$ Hz is plotted in Figure 14A; in the limit, $\nu_E \to 0$, $g_{II} \to g_c$, where g_c is the critical value of the I-I coupling at which the AS would lose stability in the inhibitory population if it were isolated from the excitatory population. This is expected since in this limit, the excitatory population has no effect because it is inactive. In the limit of large ν_E, also, $g_{II} \to g_c$. This is because in this limit, the modulation of the excitatory drive on the inhibitory population becomes small, and therefore the excitatory population has no dynamical effect on the inhibitory population. For intermediate values of the excitatory firing rate, g_{II} is a nonmonotonic function of ν_E. The minimum value is reached for $\nu_E \approx \nu_I$. It is about 25% more negative than g_c. Note that the position and the maximum of g_{II} depend on ν_I. As a rule, we have found that when ν_I is large, this maximum is more pronounced, and it is located around a value of $\nu_E < \nu_I$ as depicted in Figure 14A. These results show that in general, the feedback between the two populations disrupts the emergence of synchrony through the mutual interactions between the inhibitory neurons unless the average frequencies of the two populations differ sufficiently.

The frequencies of the two populations affect the instability on L4 in a different way, as shown in Figure 14B. Here, we have plotted the critical value of the feedback, $-g_{EI}g_{IE}$, between the two populations versus the frequencies ν_E and ν_I for $g_{EE} = g_{II} = 0$. The feedback required to destabilize the AS is minimum, around $\nu_E = \nu_I \approx 27.5$ Hz. Note that this minimum is deep but that its curvature is small. Therefore, in contrast to what happens on L2, synchrony is favored on L4 if the average frequencies in the two populations are similar. The behavior for line L3 is similar to the one found for L4. The critical value of the feedback is smaller when the two populations have the same firing rate. However, in this case, the system is much more sensitive to the difference in the firing rates. For instance, a factor of 2 between ν_E and ν_I generates an increase of a factor of 10 in the critical

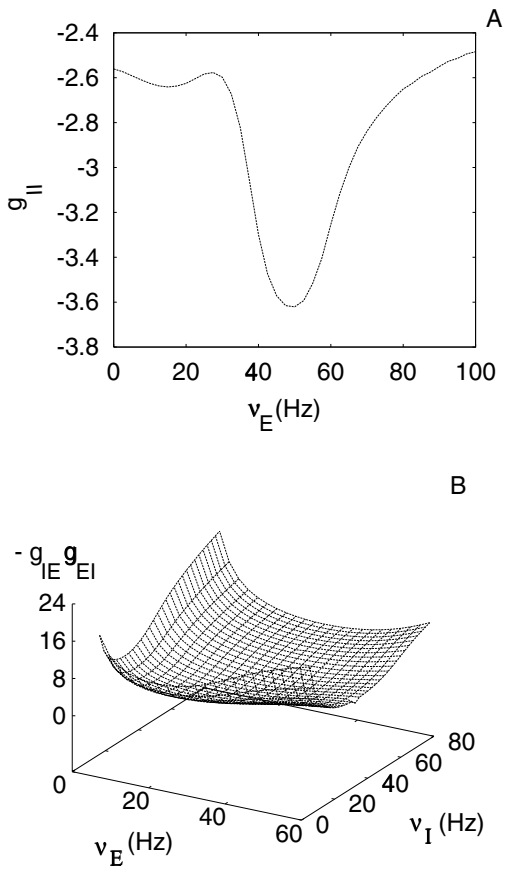

Figure 14: (A) The strength of the mutual inhibition, g_{II}, for which the AS becomes unstable on line L2 versus the average frequency of the excitatory population, ν_E. The average frequency of the inhibitory population is $\nu_I = 50$ Hz. Other parameters are $g_{EE} = 2$ and $g_{EI}g_{IE} = -4$. (B) $-g_{EI}g_{IE}$ versus the average firing rates of the two populations for which a Hopf bifurcation (L4) occurs. Here, $g_{EE} = g_{II} = 0$. In A and B, the synaptic time constants are $\tau_{1E} = \tau_{1I} = 1$ msec, $\tau_{2E} = 3$ msec, $\tau_{2I} = 6$ msec and the standard deviations of the input distributions are $\sigma_E = \sigma_I = 0.2$.

$-g_{EI}g_{IE}$ (data not shown here), while the change on L4 is less than 100%. This behavior is similar to the one found in the previous section: line L3 is a much less robust transition than line L4.

6 Numerical Simulations

The study of the solutions of equation 3.16 has allowed us to determine in the parameter space the AS stability region and the different ways this state can become unstable. The goal of this section is to complete the characterization of these instabilities and the patterns of synchrony that emerge beyond their onset. We focus on the following questions:

- Are the transitions at the onset of instabilities sub- or supercritical when they occur through a Hopf bifurcation?
- To what extent is the imaginary part of the unstable eigenvalue on the instability lines a good estimator of the frequency of the population in the stable oscillatory state in which the network settles beyond but close to these lines? Is the phase lag, δ, computed from the linearized dynamics, a good estimator for the actual phase lag between the oscillations of the activities in the two populations in the stable state near the instability onset? The answer to these two questions depends critically on the nature of the Hopf bifurcation.
- Which one of the excitatory or inhibitory populations is more synchronized near onset of synchrony? How can their relative level of synchrony be controlled?

In principle, the answer to the first question can be determined analytically by expanding the dynamics beyond the linear order. However, this calculation is extremely involved and is beyond the scope of this article. Therefore, to clarify all these issues, we relied on numerical simulations. These were performed by integrating the dynamics of the network using a second-order Runge-Kutta scheme with a fixed time step, $dt = 0.1$ msec. This algorithm was supplemented by an interpolation for the determination of the firing times of the neurons (Hansel, Mato, Neltner, & Meunier, 1998; Shelley & Tao, 2001).

6.1 The Nature of the Hopf Bifurcations. In a subcritical Hopf bifurcation, the stable fixed point, a stable limit cycle, and an unstable limit cycle can coexist in some range of the control parameter near the onset of bifurcation. This does not happen if the bifurcation is supercritical. One can use this criterion to characterize the nature of a Hopf bifurcation in numerical simulations by checking whether the system displays a hysteresis when the control parameter is changed continuously from a value where only the fixed point exists up to values where only the limit cycle is stable and backward.

We performed numerical simulations in the vicinity of the three lines L2, L3, and L4. The state of the network was characterized by computing the synchrony level χ in the two populations, as explained in appendix C. Simulations with different network sizes were compared to check that syn-

chrony was not due to a finite-size effect. An example of the results of this study is shown in Figures 6.1A through 15C for $\sigma = 0.1$ and network size $N_E = N_I = 12,560$ near instability points chosen on L2, L3, and L4, respectively. No hysteresis is apparent in the vicinity of the instability points on L2 (see Figure 15A). Although a small hysteresis cannot be completely excluded, our simulations were unable to detect it. In contrast, near L3 and L4,

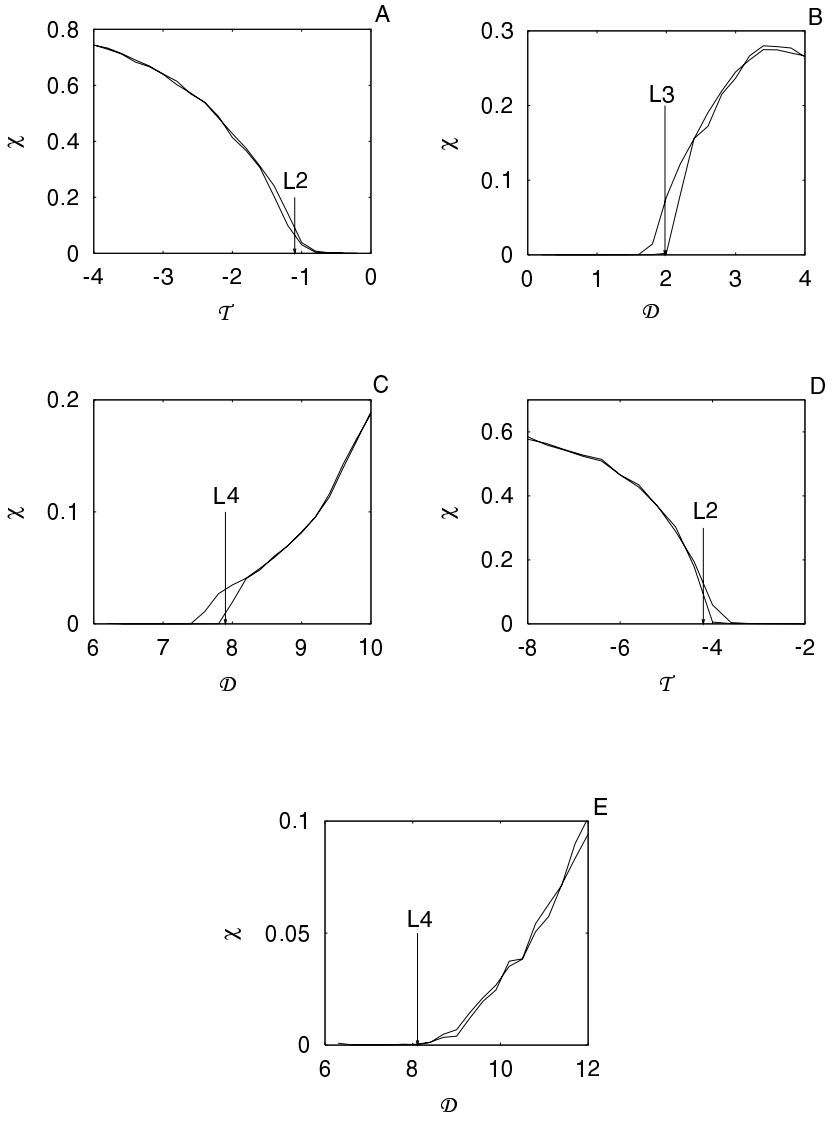

the network displays some hysteresis (see Figures 15B and 15C). However, this is a small effect since the range of coupling strength in which it occurs, as well as the value of the synchrony parameters, χ, on the left branches of the hysteresis, are small.

When σ increases, a hysteresis also appears near the instability points on L2. This effect can be seen by comparing Figures 15A and 15D, which were obtained for $\sigma = 0.1$ and $\sigma = 0.4$, respectively. However, this is a small effect, which can hardly be distinguished from sample-to-sample fluctuations if the network size is too small (result not shown). Near L4, for this value of σ, the hysteresis has shrunk and cannot be seen.

6.2 The Frequency of the Synchronous Oscillations and the Phase Lag Between the Two Populations. Our simulations indicate that a supercritical Hopf bifurcation occurs on L4 for large levels of heterogeneities. Therefore, one expects that the pattern of synchrony should be correctly predicted by our linear stability analysis near the bifurcation. This is confirmed in Figure 16A, where simulation results for the frequency of the population oscillations near L4 are plotted for the parameters of the phase diagram in Figure 7.

The simulations were performed along a line parallel to line L4, and the results are compared with the value predicted from a linear stability analysis. In Figure 17A, the potentials of one excitatory neuron and one inhibitory neuron are plotted for $\mathcal{T} = 5.25, \mathcal{D} = 8$. On this point, the global frequency is much smaller than the firing rate of the neurons. This means that the system must be bursting, as observed in the simulation.

Figure 15: *Facing page*. The level of synchrony in the excitatory population close to the Hopf bifurcations lines in the symmetric case. For each value of the bifurcation control parameter (corresponding to the x-axis), the network was simulated during 60,000 time steps. At the end of the run, the final state of the network was kept and used as initial conditions to run a new simulation after the control parameter was incremented. In each figure, two lines are shown. One corresponds to a sweep positive increment and the other to a negative increment. The standard deviation of the input is $\sigma = 0.1$ (A) The strength of the recurrent excitation is fixed $g_{EE} = 2$ and g_{II} was changed. For each value of g_{II}, $g_{EI}g_{EI}$ is varied to keep $\mathcal{D} = 0$. Predicted transition on L2 at $\mathcal{T} = -1.11$ (vertical arrow). (B) The E-E and I-I couplings are fixed: $g_{EE} = g_{II} = 0$. The E-I and I-E coupling are varied with $g_{EI} = -g_{IE}$. Predicted transition on line L3 at $\mathcal{D} = 1.98$ (vertical arrow). (C) The E-E and the I-I interactions are fixed, $g_{EE} = 5$, $g_{II} = 0$ and g_{EI} and g_{IE} are changed simultaneously with $g_{EI} = -g_{IE}$. Predicted transition on L4 at $\mathcal{D} = 7.9$ (vertical arrow). (D) g_{II} and g_{EI}, g_{IE} are changed such that $g_{EI} = -g_{IE}$ and $\mathcal{D} = -1$. Predicted transition on L2 at $\mathcal{T} = -4.2$ (vertical arrow). (E) The E-E and the I-I interactions are fixed: $g_{EE} = g_{II} = 0$ and g_{EI} and g_{IE} are changed simultaneously with $g_{EI} = -g_{IE}$. Predicted transition on L4 at $\mathcal{D} = 8.11$.

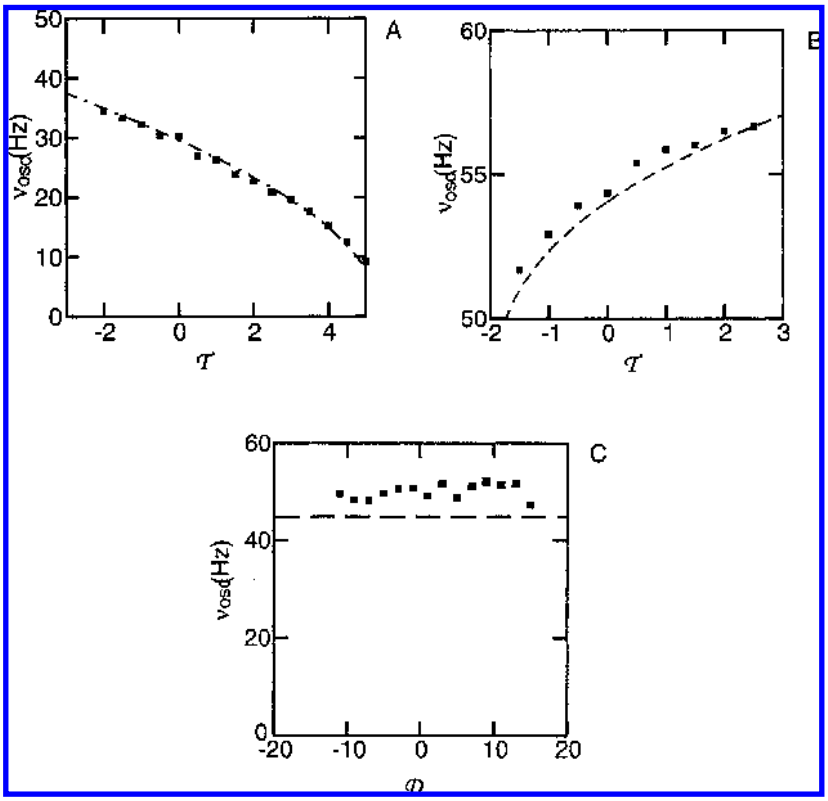

Figure 16: The frequency of the population activity oscillations near the onset of instability of the AS. The lines represent the predicted frequency from the solution of the spectral equation, equation 3.16. The squares are the results from simulations. A network of $N_E = N_I = 1600$ was simulated during 60,000 time steps and the frequency oscillation was obtained by evaluating the autocorrelation of the average membrane potential. (A) Parameters as in Figure 7. The simulations were done near L4 at distance 2 away from L4 with $g_{IE} = -g_{EI}$ and keeping $g_{II} = -2$. (B) Parameters as in Figure 4. The simulations were done at a distance 1 away from line L3 with $g_{IE} = -g_{EI}$ and keeping $g_{II} = -2$. (C) Parameters of Figure 7. The simulations were done at a distance 2 away from line L2 varying $g_{IE} = -g_{EI}$ and keeping $g_{EE} = 0$.

The Hopf bifurcations that occur on L3 (for small levels of heterogeneities) as well as on L2 if the level of heterogeneities is sufficient were found to be subcritical. Therefore, one expects that the actual oscillation frequencies and phase lags near these lines should deviate from the values obtained for the

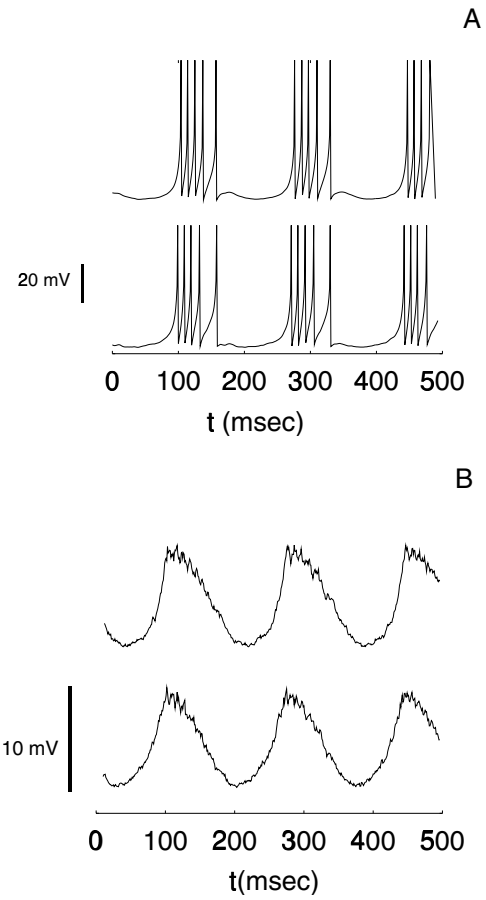

Figure 17: Synchronous oscillations in which neurons fire bursts of spikes. Parameters as in Figure 7 with $\mathcal{T} = 5.25$ and $\mathcal{D} = 8$. (A) Excitatory neuron (lower trace) and inhibitory neuron (upper trace). (B) The membrane potential of the excitatory (resp. inhibitory) neurons averaged over all the population (lower line, resp. upper line).

unstable mode in the linear stability analysis. In spite of this, a reasonable agreement between the predictions and the simulation values was found as shown in Figures 16B and 16C. This is because the hysteresis near L2 has a small range and a small amplitude (see, e.g., Figure 15B).

In Figure 6, the phase lag between the oscillations of the activity of the two populations is plotted as a function of g_{EE} for $g_{II} = 0$ (A) and as a function of g_{II} for $g_{EE} = 0$ (B). The solid and dashed lines correspond to the predictions from our analytical results. Results from numerical simulations

performed in the vicinity of the instability lines are represented by squares. They were estimated from the position of the cross-correlation peak of the activities of the two populations. In agreement with the linear theory, the phase lag on L3 and L4 are nonmonotonic functions of the coupling. For instance, on line L4, it reaches a maximum of $\pi/2$ when $g_{EE} = g_{II} = 0$ and then decreases as one approaches points B or D in the phase diagram. The negative sign of the phase lag means that the oscillation of the activity of the excitatory population is ahead of the inhibitory one. Note that on L3, the lag has the opposite sign, that is, the inhibitory population oscillates ahead of the excitatory one. On line L4 near D, the linear theory predicts that the phase lag should become small and vanish at D. This is confirmed by our numerical simulations, as shown in Figure 17B.

Finally, the linear theory predicts that at the instability onset on L2, the phase lag should be zero. Therefore, δ is expected to be small near L2 when synchrony occurs. Our simulations are in line with this prediction.

6.3 The Level of Synchrony in the Two Populations. For strong enough g_{II}, the activity of the inhibitory neurons can synchronize as a result of their mutual coupling. If the feedback between the two populations, $-g_{EI}g_{IE}$ is weak, the dynamical state of the inhibitory population should not be perturbed much. However, the excitatory population is now entrained by the inhibitory one. Therefore, it develops synchrony. The level of synchrony in the excitatory population depends on the coupling g_{EI}. For small g_{EI}, one expects the excitatory population to be weakly synchronized, and the level of synchrony should increase with g_{EI}. These expectations were confirmed by our numerical simulations. Moreover, under these conditions, the inhibitory population was always substantially more synchronized than the excitatory one (results not shown). More generally, we found this property to be true in the vicinity of L2 even for large values of $-g_{EI}g_{IE}$. This can be seen in Figure 18, where the synchrony measures, χ_E and χ_I, are plotted against $-g_{IE}g_{EI}$, for $g_{EI} = -g_{IE}/4$ (A) and for $g_{EI} = -4g_{IE}$ (B). In both cases, the transition point on L2 occurs for the same value of $-g_{IE}g_{EI}$, namely, $-g_{IE}g_{EI} \approx 3.25$. This agrees with the fact that the spectral equation depends on only g_{EI} and g_{IE} through their product. However, the level of synchrony in the two populations also depends on the ratio g_{EI}/g_{IE}. On both curves, the inhibitory population is always more synchronized than the excitatory one. The synchrony in the excitatory population varies nonmonotonically with $g_{EI}g_{IE}$, with an intermediate region where the AS is stable. This is because the feedback between the two populations has two opposing effects. On the one hand, it drives the excitatory population, and on the other, it disrupts the synchrony induced by the mutual I-I interactions in the inhibitory population. Finally, increasing g_{EI} (for fixed $g_{EI}g_{IE}$) increases χ_E. This is because the larger the $|g_{EI}|$, the stronger is the inhibitory drive on the excitatory population.

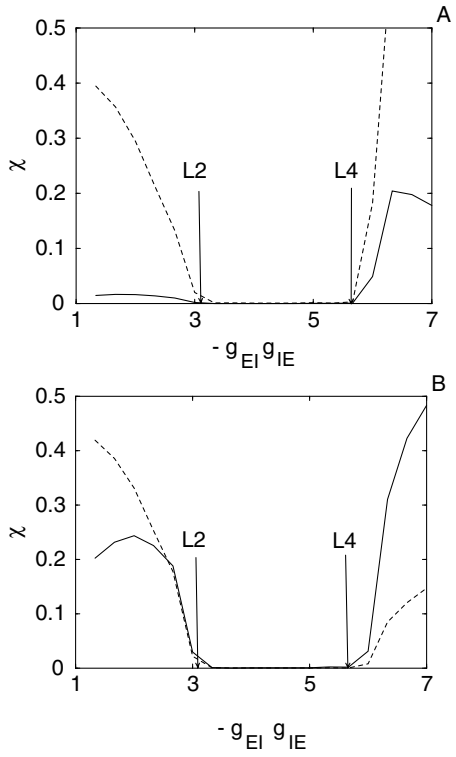

Figure 18: The synchrony level of the excitatory (solid line) and the inhibitory populations (dashed line) versus $-g_{EI}g_{IE}$. The strength of the E-E and I-I interactions are fixed: $g_{EE} = 2$, $g_{II} = -2$. Other parameters $\nu_E = \nu_I = 50$ Hz, $\sigma_E = \sigma_I = 0.2$. A network with $N_E = N_I = 1600$ neurons was simulated for different values of g_{EI} and a fixed ratio g_{EI}/g_{IE}. (A) $g_{EI}/g_{IE} = -1/4$. (B) $g_{EI}/g_{IE} = -4$. The level of synchrony was calculated as explained in appendix C (average over 6 seconds). The theory predicts that the AS becomes unstable at $-g_{EI}g_{IE} = 3.25$ (on L2) and $-g_{EI}g_{IE} = 5.7$ (on L4) as indicated by the arrows.

In all our numerical simulations, we found that in the vicinity of L2, the level of synchrony is larger in the inhibitory population than in the excitatory one. This is in contrast with what happens near L3. This is shown in Figure 19. Here, for a given value of $-g_{EI}g_{IE}$, the relative level of synchrony depends strongly on the balance between g_{EI} and g_{IE}. For large g_{EI} and small g_{IE}, the synchrony in the excitatory population is higher than in the inhibitory one. The opposite happens if g_{IE} is large and $|g_{EI}|$ is small. The same figure also shows that the synchrony levels near line L4 are affected in the same way by the balance between g_{EI} and g_{IE}. Making the excitatory to

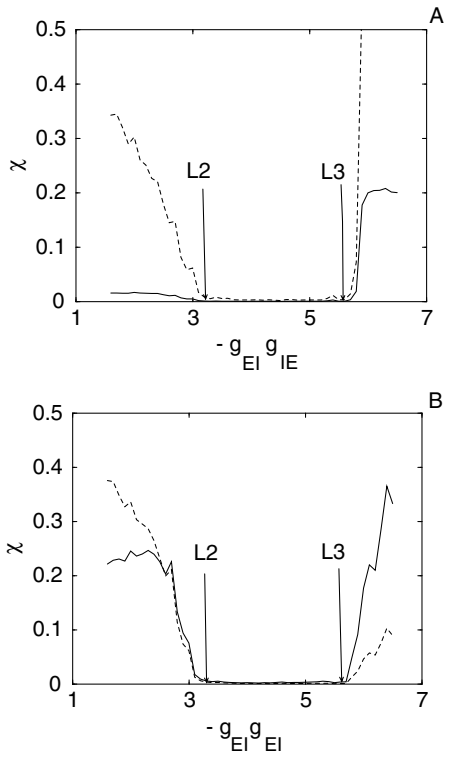

Figure 19: The synchrony level of the excitatory (solid line) and the inhibitory populations (dashed line) vs. $-g_{EI}g_{IE}$. The strength of the E-E and I-I interactions is fixed: $g_{EE} = 2$, $g_{II} = -2$. Other parameters $\nu_E = \nu_I = 50$ Hz, $\sigma_E = \sigma_I = 0.1$. A network with $N_E = N_I = 1600$ neurons was simulated for different values of g_{EI} and a fixed ratio g_{EI}/g_{IE}. (A) $g_{EI}/g_{IE} = -1/4$ (B) $g_{EI}/g_{IE} = -4$. The level of synchrony of the two populations was calculated as explained in appendix C (average over 6 seconds). The theory predicts that the AS becomes unstable at $-g_{EI}g_{IE} = 2.96$ (on L2) and $-g_{EI}g_{IE} = 5.42$ (on L3) as indicated by the arrows.

inhibitory interaction stronger makes the inhibitory population more synchronized, and vice versa.

7 Discussion

In this work, we have analyzed the synchronization properties of a fully connected two-population system. We have not intended to present a complete model of the cortex, but a simple network model that is amenable to analytical treatment. A natural but nontrivial extension of our work would

be to study the stability of asynchronous states in networks with more structured patterns of connectivity such as the ones found in the visual cortex, which include local or intracolumnar connections between neurons with similar feature preference, vertical connections between different layers, and feedback connections from higher cortical areas. For instance, one expects that in a network with space-dependent interactions, instabilities of the AS may lead to traveling waves or other spatiotemporal patterns in which hot spots of activity move across the system (Ben Yshai, Hansel, & Sompolinsky, 1997; Hansel & Sompolinsky, 1998; Golomb, 1998; Golomb & Ermentrout, 1999).

7.1 Three Mechanisms for Synchrony in Two-Population Networks.

7.1.1 The Mutual Inhibition Mechanism. The activity of inhibitory neurons can be synchronized on the timescale of the spikes through their mutual interactions. It has been proposed that hippocampal γ rhythms can be driven by populations of inhibitory interneurons whose activity is synchronized through this mechanism (Buzsáki & Chrobak, 1995). Synchrony in one population of inhibitory neurons has been extensively studied in recent years theoretically (van Vreeswijk, Abbott, & Ermentrout, 1994; Hansel, Mato, & Meunier, 1995; van Vreeswijk, 1996; Wang & Buszáki, 1996; White et al., 1998; Chow, 1998; Chow, White, Ritt, & Kopell, 1998; Golomb & Hansel, 2000; Neltner et al., 2000; Whittington, Traub, Kopell, Ermentrout, & Buhl, 2000) and experimentally (Whittington, Traub, & Jefferys, 1995; Traub, Whittington, Colling, Buzsáki, & Jefferys, 1996; Traub, Jefferys, & Whittington, 1999, for a review). Here, we have generalized this mechanism to take into account the effect of a second excitatory population. When the cross-talk interaction between the two populations is not too large, we have found that the AS becomes unstable if the mutual inhibition is sufficiently strong. Excitation plays against this destabilization in two ways. For a given value of the feedback between the two populations (fixed value of $|g_{EI}g_{IE}|$), the strength of the mutual inhibition g_{II} required to destabilize the AS increases with g_{EE}. Also, for a given g_{EE}, a larger mutual inhibition is required if the feedback between the two populations is increased. If $|g_{EI}g_{IE}|$ is too strong, another mechanism for the destabilization of the AS can occur, as discussed below. These desynchronizing effects of the excitatory population are stronger when the average firing rates of the two populations are more similar. In the example shown in Figure 14, $|g_{II}|$ is maximal when the firing rates of the two populations are similar. Therefore, as far as the value of g_{II} is concerned, the excitatory population has a strong influence. In contrast, we have found that the frequency of the unstable mode at the transition is mainly determined by the average firing rate of the inhibitory population and depends only weakly on the properties of the excitatory population and on the way the two populations interact. Related to this fact, we have shown that the phase shift between the two populations is very small even

if their average firing rates are very different. In view of these features, this mechanism can arguably be based on the synchronization of the inhibitory population.

Our analysis focuses on the mechanisms for destabilization of the AS. We address this problem by studying local bifurcations of the AS. Therefore, we did not address the issue of rhythm properties under strong synchrony. Strongly synchronized states could coexist with the weakly synchronous states or even the AS. The only way to address this question (and the question of the size of the attraction basins of the stable states) is with extensive numerical simulations. The fact that the frequency of the unstable mode is determined to a large extent by the average firing rate of the neurons in the AS does not contradict previous results indicating that when the synchrony is substantial, the rhythm frequency can depend on the synaptic time constant of mutual inhibition (Whittington et al., 1995; Chow et al., 1998; White et al., 1998).

7.1.2 The Cross-Talk Mechanisms. We have demonstrated that the AS can be destabilized with two qualitatively different mechanisms by the cross-talk interactions between the two populations.

In the first mechanism (on L4), the inhibitory population lags behind the excitatory one. Therefore, in the unstable mode, an increase in activity of the excitatory population makes the inhibitory neurons increase their activity. This generates in return an increase in inhibition of the excitatory neurons, which tends to prevent simultaneous firing of many of these neurons. Sufficiently strong feedback between the two populations will prevent the perturbation from decaying, and synchrony will emerge. Mutual excitation of excitatory neurons favors the development of this instability since it helps to amplify perturbations in the E population. Mutual inhibition of inhibitory neurons disrupts the development of this instability since it reduces the excitability of this population. In this mechanism, synchrony is induced by recurrent inhibition of the excitatory population. It has been investigated mostly by numerical simulations in previous studies and has been proposed as a mechanism for γ oscillations (Jefferys, Traub, & Whittington, 1996). However, as shown here, this mechanism can lead to slow oscillations. The oscillations can be so slow that the neurons develop bursts of action potentials.

In the second type of cross-talk instability (on L3), the inhibitory population tends to fire in advance with respect to the excitatory one, preventing the excitatory neurons from firing. In return, this deexcitation reduces the activity of the inhibitory neurons. This instability does not decay provided that the feedback between the two populations is sufficiently strong. The global oscillations near this instability are on the order of or faster than the average firing rate of the neurons.

These two mechanisms are qualitatively different from the mutual inhibition mechanism. Indeed, we have found that the frequency of population

activity as well as the phase shift between the oscillations in the two populations vary substantially and continuously on the corresponding instability surfaces. Also, the emerging oscillations in the two populations can display a large phase shift, δ. However, in all the examples we have studied, the numerical solution of the spectral equation reveals that $|\delta| < \frac{\pi}{2}$. We did not prove this statement in general. However, we have proved that in the symmetric case, $|\delta| = \pi/2$ on onset instability lines L3 and L4 at $g_{EE} = g_{II} = 0$. We have also shown that δ has a local maximum at that point. Without the assumption of symmetry between the two populations, we have also shown that the oscillations of the two populations become in phase when the emerging rhythm becomes very slow.

7.1.3 Robustness of Synchrony to Heterogeneities. A systematic and comparative study of the robustness of the various modes of destabilization would be a very tedious task. Nevertheless, some general trends emerge from the study of the spectral equation in the symmetric case. The coupling strengths required for destabilization on L2 and L3 depend crucially on the heterogeneity level (see Figure 9). This is in contrast with what happens for L1 and L4 where the dependence is much weaker. Thus, the recurrent inhibition is the most robust mechanism for synchronous oscillations. Another difference between line L3 and the other lines is that for sufficiently large σ, L3 lies completely inside a region, which is beyond instability line L4. Therefore, when the level of heterogeneities increases, this line becomes physically irrelevant. In this sense, the mechanism corresponding to this instability line is much less robust than the other mechanisms. Similar trends were also found in all the examples we investigated after relaxing the symmetry assumption.

Recent studies have suggested that because of heterogeneities, synchrony in inhibitory networks can be difficult to achieve (White et al. 1998; Chow et al., 1998). Our study provides an example of a model in which the desynchronizing effect of large levels of heterogeneities can be overcome provided that the external excitatory drive and the synaptic interactions are sufficiently strong. Simulation results in the framework of a conductance-based model were found to be consistent with this conclusion (Neltner et al., 2000). This is in contrast with the behavior of inhibitory networks of leaky integrate-and-fire models where for sufficiently large level of heterogeneities, the AS is always stable (Golomb et al., 2001). For sufficiently strong coupling, the AS is stable even if the network is homogeneous. This is yet another difference with the present model. Below, we elaborate further on these differences.

7.2 Getting Rid of Synchrony. The frequent occurrence of synchronous neuronal activity in physiopathological states in the brain (see Bergman et al., 1998; McCormick & Contreras, 2001) suggests that in many situations, synchronous states of activity need to be prevented. The issue is to understand how synchrony can be prevented in particular in systems

where massive feedback interactions are observed. Our analysis shows that even if the interactions are strong, a suitable balance between excitation and inhibition stabilizes the AS. We have proved this statement for our model in full generality and analytically under the assumption of symmetry between the two populations. Indeed, for $\mathcal{D} = \mathcal{T} = 0$, the AS is marginally stable without heterogeneities, and it becomes stable when heterogeneities are added. Besides the presence of heterogeneities, this implies that if the excitatory feedback connections, g_{EE}, are strong, the two populations must interact strongly, and the mutual interactions of the inhibitory neurons must be strong to ensure that the AS is stable. In particular, if g_{II} is not strong enough, the system tends to fire synchronous bursts. Increasing g_{II} reduces the excitability of the inhibitory population, preventing the synchronous bursts from developing. This desynchronizing effect of mutual inhibition also holds in the nonsymmetric case, as shown in Figure 11.

7.3 Application to the Stability of Persistent Activity. Hebb (1949) proposed that the representation of an object in short-term memory consists of the set of cortical cells that this object activates when it is presented. According to this hypothesis, the reverberation of excitation across this set is able to maintain activity even when the stimulus has been removed, thus preserving a memory of the object. In other words, the network displays multistability. The fact that persistent activity requires strong excitatory feedback poses the problem of control of neural activity in persistent states at firing rates in the range 10 to 30 spikes per second, as observed in experiments. Wang (1999) has argued, mostly on the basis of numerical simulations, that to achieve a stable persistent state with activities in a physiological range (10–50 Hz), recurrent excitatory synapses must be dominated by a slow component. It was subsequently proposed that NMDA synapses were required to achieve such states. Another possibility is that inhibition controls the firing rate (Rubin and Sompolinsky, 1989). However, recurrent inhibition can also induce synchrony, and this can be incompatible with low rate persistent activity. Indeed, if the neurons fire synchronously in some short time window, the fast excitatory feedback will decay before the neurons fire their next spike. Note, however, that weak synchrony may be compatible with persistent activity.

The results shown in Figure 12 indicate that strong mutual inhibitory interactions with synaptic time constants in a range corresponding to $GABA_A$ synapses stabilize the AS even if the recurrent excitation is mediated by nonsaturating AMPA synapses. Therefore, strong $GABA_A$ mutual inhibition should help achieve a stable persistent state. This is in line with the conclusions of our previous study (Hansel & Mato, 2001), in which the threshold distribution had a finite support. Here, we show that this is true for a gaussian distribution of threshold without truncation (see Figure 3).

At first glance, this contradicts the results of Wang (1999). However, I-I interactions were not included in Wang's study. This may explain why it concluded that stable persistent activity was impossible to achieve with AMPA excitatory synapses and that NMDA synapses were necessary. One should note that recent anatomical and physiological studies have revealed that I-I connections are numerous and strong in the cortex (Sik, Penttonen, Ylinen, & Buzsáki, 1995; Tarczy-Hornoch, Martin, Jack, & Stratford, 1998; Gupta, Wang, & Markram, 2000). The role we suggest for these connections in the stability of persistent activity fits nicely with these experimental results, without excluding that NMDA synapses could also contribute to delay period activity in cortex.

7.4 Comparison with Networks of Leaky (Linear) Integrate-and-Fire Networks. In the absence of noise, a very precise fine tuning of the external input is required to get a LIF neuron to fire below 8 spikes per second. This is due to the logarithmic behavior of the ν-I curve near current threshold. Furthermore, there is an exponential divergence of the function $H(\nu)$ (the equivalent of equation 3.18 for the leaky integrate-and-fire neuron; Golomb et al. 2001) when $\nu \to 0$ unless $P(x)$ vanishes at least exponentially fast when $x \to 0$. In this situation, U also diverges, and the spectral equation is not well defined. This divergence is due to the fact that at very low rates, the LIF model spends an exponentially long time near the threshold. This is because leaky integrate-and-fire neurons integrate their inputs in a purely passive way. As a consequence, if the external currents the neurons receive are distributed according to a gaussian, the resulting distribution of firing rate does not vanish sufficiently fast at zero firing rate for the integrals in $H(\nu)$ to converge. To avoid this problem, a gaussian distribution of period was chosen in Golomb et al. (2001). In contrast, for the QIF model in the limit of very low rates, $H(\nu)$ goes as $(\exp(-\lambda/\nu)-1)P(\nu)/\nu$. Therefore, in this limit, U is proportional to the average period of the population, which is defined even if the distribution of firing rates does not vanish at zero frequency.

Another difference between the two models is that in LIF inhibitory networks, instability of the AS can lead to cluster states (van Vreeswijk, 1996; Neltner et al., 2000; Golomb & Hansel, 2000). The number of clusters thus generated can be rather large, especially at low firing rates. This does not happen in our model, since the numerical solution of the spectral equation reveals that the onsets to clustering instabilities are always within the regions where the AS is already unstable. These instabilities are therefore irrelevant for the AS. Of course, this does not exclude the possibility that clustering occurs far from the onset of the instabilities in our model as well. The origin of this different behavior can be clarified in the weak coupling limit. In this limit, the instabilities of the AS can be related to the Fourier expansion of the response function, $Z(\phi)$, of the neurons, where ϕ is the phase variable describing the position of the neuron on its limit cycle (Kuramoto, 1984; Neltner et al., 2000). Destabilization of the AS through an n-cluster

instability mode in a heterogeneous network requires a large Fourier coefficient of order n. In the LIF model, the function Z is an exponential and is discontinuous at $\phi = \pi/2$. Therefore, all the Fourier coefficients are large and even diverge in the limit of small firing rates. One can further show that in this limit, the order of the unstable leading mode increases. In contrast, for the QIF, the amplitude of the response function diverges but proportionally to $\cos(\phi)$ (up to a constant). Therefore, the dominant mode becomes the first one. This difference has its origin in the way the membrane potential approaches the threshold potential at low rate. In the LIF the derivative of the membrane potential that is just before the spike threshold goes to zero with the firing rate. This is not the case for the QIF where this derivative is proportional to $V_t^2 \neq 0$.

7.5 Relation to Previous Studies. Mechanisms of neuronal synchrony have been addressed in recent years, following two different and complementary theoretical approaches. One has been to study the conditions under which fully synchronized states or more general phase-locked states are stable in fully connected networks of identical neurons (Wang & Rinzel, 1992; Hansel, Mato, & Meunier, 1993b; van Vreeswijk et al., 1994; Hansel, et al., 1995; White et al., 1998; Chow, 1998; Crook, Ermentrout, & Bower, 1998). The other approach has been to investigate the conditions of the stability of the asynchronous state of a large neuronal system (Abbott & van Vreeswijk, 1993; Gerstner & van Hemmen, 1993; Treves, 1993; van Vreeswijk, 1996, 2000; Brunel & Hakim, 1999; Brunel, 2000; Golomb & Hansel, 2000; Neltner et al., 2000; Gerstner, 2000). The latter approach was followed here.

This article aims to contribute to a comprehensive understanding of the patterns of synchrony in two-population heterogeneous neuronal networks with full connectivity. In order to make the model more amenable to analytical calculations, noise was not introduced. An expected consequence of adding input noise is to increase the parameter domain where the AS is stable. Still, if the noise is not too strong, simulations indicate that three instabilities may occur for the AS. However, another type of instability can also be found if the noise is strong enough. It leads to a state in which the population oscillations are faster than the average firing rate of the neurons. In this state, the firing pattern of the neurons can be very irregular, and averaging over a large number of neurons is necessary to reveal the existence of the underlying rhythmic component in the network activity. Such patterns of synchrony, called fast oscillations, were studied first by Brunel and Hakim (1999) in sparse networks of inhibitory leaky integrate-and-fire neurons. The results of this study were subsequently generalized to the case of two populations with sparse connectivity (Brunel, 2000; N. Brunel, C. Geisler, & X.-J. Wang, private communication Dec. 2001). More recently, Brunel and Hansel (2002) have shown that sparse connectivity was not required for fast oscillations to take place but that they can occur in a fully connected network of inhibitory neurons in the presence

of strong input noise. Increasing the coupling destabilizes the AS, leading to a state where the neurons fire synchronously at a rate that can be significantly smaller than the population oscillations. Therefore, when noise is also present, the AS can become unstable through four generic mechanisms.

The all-to-all connectivity considered here can be thought of as the extreme case of a system in which the connectivity is high. Indeed, we have checked that our results still hold when the connectivity is random and sufficiently dense (results not shown). However, an important difference exists between the collective behavior of densely and sparsely connected networks. In densely connected networks in the absence of input noise, the neurons discharge in a very regular manner. This is because the fluctuations in the synaptic input are small—of the order of $O(1/K)$, where K is the connectivity. In contrast, in sparse networks with strong excitatory and inhibitory synapses, the firing of the neurons can be highly irregular even if no input noise is present (van Vreeswijk & Sompolinsky, 1996, 1998; Brunel, 2000). In this state, the stochasticity of the firing is of deterministic origin, and the fluctuations in the synaptic input remain large due to a balance between excitation and inhibition.

We have shown that in the presence of an excitatory population, a stronger coupling is required to synchronize activity through mutual inhibition. A similar conclusion was reported in Traub, Jefferys, and Whittington (1997) relying on a simulation of a detailed conductance-based model. These authors found that excitation can destroy a synchronous state generated by mutual inhibition. We should also remark that the desynchronizing effect of excitation is a characteristic feature of type I neurons. For type II neurons (such as in the Hodgkin-Huxley model), excitation can have a strongly synchronizing effect, especially at low firing rates (Hansel, Mato, & Meunier, 1993b; Hansel et al., 1993a, 1995).

The fact that mutual inhibition can prevent recurrent inhibition to induce synchrony was noted by Tsodyks, Skaggs, Sejnowski, and McNaughton (1997) in the framework of a two-population rate model. In this work, strengthening the I-I interactions was shown to prevent the two populations from developing synchronous oscillatory rate modulations. Since we have seen that in the limit of infinitely slow synapses, the spectral equation becomes equivalent to the spectral equation of a rate model, it is not surprising that in that limit, our conclusions agree with the results of Tsodyks et al. (1997). However, mutual inhibition is a powerful way to generate synchrony on a timescale comparable to the timescale of AMPA and $GABA_A$ interactions. Therefore, it was not clear a priori that this mechanism would still hold for these synapses. Our detailed stability analysis of the AS shows that this is indeed the case.

A desynchronizing effect of mutual inhibition was also reported by Bush and Sejnowski (1996) in simulations of a two-population model of a column in primary visual cortex. It was found that when the inhibition between the

basket cells is increased, the temporal modulation of the local field potential is decreased and the neurons are less bursty. However, in this work, the firing rate of the neurons changed when the mutual inhibition was increased. Another difference with our work is that in the simulations presented by Bush and Sejnowski, the neurons were intrinsic bursters. Therefore, in their case, the desynchronizing effect of mutual inhibition could also have been the consequence of a disruption of the intrinsic bursting when the inhibitory synaptic input became stronger.

Excitatory cells in cortex display strong spike adaptation, whereas interneurons do not. To reduce the number of parameters of our two-population model, we assumed the dynamics of the two populations were identical and spike adaptation was not introduced in the excitatory dynamics. Recent theoretical studies have investigated the dynamics of excitatory networks of neurons with spike adaptation (van Vreeswijk & Hansel, 2001; Fuhrman, Markram, & Tsodyks, 2002). In these works, it was demonstrated, mostly analytically, that excitation and spike adaptation can cooperate to create synchronous oscillatory activity and that the frequency of these oscillations depends on the kinetics of the adaptation process. In particular, if the excitatory recurrent feedback and the adaptation is sufficiently strong and slow, the network settles into a state in which the neurons fire synchronous bursts (van Vreeswijk & Hansel, 2001). How an additional population of inhibitory neuron modifies this type of synchronous state was subsequently studied, relying on numerical simulations (van Vreeswijk & Hansel, 2001). The main conclusion was that recurrent inhibition of the excitatory population (E-I-E feedback loop) plays against the emergence of the synchronous bursts but that mutual inhibition (I-I interactions) favors it. In contrast, we have found in our model that recurrent inhibition favors the synchronous bursting that emerges on instability lines L3 and L4 but that mutual inhibition disrupts it. Keeping in mind that spike-to-spike synchrony can be induced by mutual inhibition, inhibitory interactions can thus have a spectrum of qualitatively different effects in two-population networks.

Appendix A: The Wang-Buszáki Model

The dynamical equations for the conductance-based neuron model used in this work are (Wang & Buszáki, 1996):

$$C\frac{dV}{dt} = I_{ext} - g_{Na}m_\infty^3 h(V - V_{Na}) - g_K n^4 (V - V_K) - g_l(V - V_l) + I_{syn} \quad \text{(A.1)}$$

$$\frac{dh}{dt} = \frac{h_\infty(V) - h}{\tau_h(V)} \quad \text{(A.2)}$$

$$\frac{dn}{dt} = \frac{n_\infty(V) - n}{\tau_n(V)}. \quad \text{(A.3)}$$

The parameters g_{Na}, g_K, and g_l are the maximum conductances per surface unit for the sodium, potassium, and leak currents, respectively, and V_{Na}, V_K, and V_l are the corresponding reversal potentials. The capacitance per surface unit is denoted by C. The external stimulus on the neuron is represented by an external current I_{ext}, and the synaptic current due to the interactions with other neurons in the network is I_{syn}. The functions $m_\infty(V)$, $h_\infty(V)$, and $n_\infty(V)$ and the characteristic times (in milliseconds) τ_m, τ_n, τ_h, are given by

$$x_\infty(V) = a_x/(a_x + b_x),\ \tau_x = 1/(a_x + b_x)$$

with $x = m, n, h$ and:

$$a_m = -0.1(V + 35)/(\exp(-0.1(V + 35)) - 1) \tag{A.4}$$

$$b_m = 4\exp(-(V + 60)/18) \tag{A.5}$$

$$a_h = 0.35\exp(-(V + 58)/20) \tag{A.6}$$

$$b_h = 5/(\exp(-0.1(V + 28)) + 1). \tag{A.7}$$

The other parameters of the sodium current are $g_{Na} = 35$ mS/cm^2 and $V_{Na} = 55$ mV. The delayed rectifier current is described in a similar way as in the HH model with

$$a_n = -0.05(V + 34)/(\exp(-0.1(V + 34)) - 1) \tag{A.8}$$

$$b_n = 0.625\exp(-(V + 44)/80) \tag{A.9}$$

and $g_K = 9$ mS/cm^2 and $V_K = -90$ mV. Other parameters of the model are $C = 1\ \mu$F/cm^2, $g_l = 0.1$ mS/cm^2, and $V_l = -65$ mV.

This neuron model displays an SN bifurcation at the current threshold to repetitive firing, I_c, in the vicinity of which the relationship between the current, I, injected in the neuron and its firing rate behaves like $f \propto \sqrt{I - I_c}$ for $I > I_c$. Therefore, they are able to fire at an arbitrarily small rate. This is also seen in Figure 1, which represents the frequency-current relation of this model.

Appendix B: Reduction of a Conductance-Based Model to the QIF Model

We consider a type I conductance-based model. The equations of the single-neuron dynamics can be written in compact form:

$$\frac{d\mathbf{X}}{dt} = \mathbf{F}(\mathbf{X}) + \mathbf{G}(\mathbf{X}). \tag{B.1}$$

In the case of the WB model, **X**, **F**, and **G** are three-dimensional vectors with:

$$X_1 = V \tag{B.2}$$

$$X_2 = h \tag{B.3}$$

$$X_3 = n \tag{B.4}$$

$$F_1(\mathbf{X}) = (I_c - g_{Na} m_\infty^3 h(V - V_{Na}) - g_K n^4 (V - V_K) - g_l(V - V_l))/C \tag{B.5}$$

$$F_2(\mathbf{X}) = (h_\infty(V) - h)/\tau_h(V) \tag{B.6}$$

$$F_3(\mathbf{X}) = (n_\infty(V) - n)/\tau_n(V) \tag{B.7}$$

$$G_1 = I - I_c \tag{B.8}$$

and $G_2 = G_3 = 0$. Following Ermentrout (1996), one can study this dynamics in the vicinity of firing onset. One writes:

$$\mathbf{G}(\mathbf{X}) = \epsilon \mathbf{N}(\mathbf{X}), \tag{B.9}$$

where $\epsilon \ll 1$. For $\epsilon < 0$, the neuron is not firing. It displays a stable fixed point: $\mathbf{X} = \bar{\mathbf{X}}(I)$. For $\epsilon > 0$, the neuron fires action potentials. At $\epsilon = 0$, a bifurcation occurs. The Taylor expansion of $F(\mathbf{X})$ around $\mathbf{X}^\star = \bar{\mathbf{X}}(I_c)$ is

$$F(\mathbf{X}) = \mathbf{F}(\mathbf{X}^\star) + \mathbf{A}(\mathbf{X} - \mathbf{X}^\star) + \mathbf{Q}(\mathbf{X} - \mathbf{X}^\star, \mathbf{X} - \mathbf{X}^\star) + \cdots \tag{B.10}$$

where **A** and **Q** are, respectively, the Jacobian and the Hessian matrices of **F** evaluated at $\mathbf{X}^\star$. Since an SN bifurcation occurs at $\mathbf{X}^\star$, the matrix **A** has one zero eigenvalue. The corresponding normalized eigenvector will be denoted by **e**. Similarly, $\mathbf{A}^T$, the transpose of **A**, has a zero eigenvalue. We will denote by **f** the corresponding eigenvector satisfying $\mathbf{f}.\mathbf{e} = 1$. For small $\epsilon > 0$, the solution $\mathbf{X}(t)$ of equation B.1 can be expanded,

$$\mathbf{X}(t) = \mathbf{X}^\star + \sqrt{\epsilon} z(t) \mathbf{e} \tag{B.11}$$

where the scalar quantity z satisfies (Ermentrout & Kopell, 1986)

$$\frac{dz}{dt} = \sqrt{\epsilon}(\eta + q z^2), \tag{B.12}$$

where: $\eta = \mathbf{f}.\mathbf{N}(\mathbf{X}^\star)$ and $q = \mathbf{f}.\mathbf{Q}(\mathbf{e}, \mathbf{e})$. This equation can easily be solved. Assuming that η and q have the same sign, one finds

$$z(t) = \sqrt{\frac{\eta}{q}} \tan \sqrt{\eta q \epsilon}(t - t_0), \tag{B.13}$$

where t_0 is a constant. Function z diverges when the argument of the tangent is a multiple of $\pi/2$. These divergences correspond to the firing of an action

potential in the original system (Ermentrout & Kopell, 1986). Therefore, in the limit $\epsilon \to 0$, the firing frequency of the neuron vanishes as

$$\nu = B\sqrt{I - I_c}, \tag{B.14}$$

with

$$B = \frac{\sqrt{\eta q}}{\pi}. \tag{B.15}$$

Coefficient B can be calculated by diagonalizing matrix A. It turns out that due to the particular structure of this matrix, expressions for $\mathbf{e}$, $\mathbf{f}$, $\mathbf{Q}(\mathbf{e}, \mathbf{e})$ can be derived analytically in terms of the gating functions (this fact has apparently escaped attention in previous papers). In particular, for the WB model, one finds that

$$\mathbf{e} = K(1, h_\infty^{'}, n_\infty^{'}) \tag{B.16}$$

$$\mathbf{f} = \frac{1}{LK}\left(1, \tau_h \frac{\partial F_1}{\partial h}, \tau_n \frac{\partial F_1}{\partial n}\right) \tag{B.17}$$

where

$$K = \frac{1}{\sqrt{1 + (h_\infty^{'})^2 + (n_\infty^{'})^2}} \tag{B.18}$$

$$L = 1 + \tau_h \frac{\partial F_1}{\partial h} h_\infty^{'} + \tau_n \frac{\partial F_1}{\partial n} n_\infty^{'}. \tag{B.19}$$

The derivative of function $f(V)$ with respect to V has been denoted $f^{'}$. In these expressions, all the functions have to be evaluated for V, n_∞, h_∞ at the fixed point of the dynamics.

Finally we find:

$$B = \frac{1}{\pi L}\sqrt{\frac{1}{2}\left(\frac{\partial^2 F_1}{\partial V^2} + 2\sum_{i=2,3} X_i^{'} \frac{\partial^2 F_1}{\partial V \partial X_i} + (n_\infty^{'})^2 \frac{\partial^2 F_1}{\partial n^2} + \sum_{i=2,3} X_i^{''} \frac{\partial F_1}{\partial X_i}\right)}. \tag{B.20}$$

The Taylor expansion of the dynamics, equation B.10, is valid in the limit of low firing rate except during an action potential where the variable z diverges. If I is sufficiently close to threshold, an approximate trajectory for the vector $\mathbf{X}(t)$ can be computed from $z(t)$ and the vector $\mathbf{e}$. This approximation is a good description of the behavior of the neuron except during the spikes, which are of short duration. It becomes exact in the limit $I \to I_c$. Therefore, near the firing onset, one can replace the full model, equation B.1, by the reduced model, equations B.11 and B.12, where all the parameters can be

computed from the full model. In particular, the shape of the f-I curve near threshold is given by equation B.14.

When $I - I_c$ is not small, this reduction is no longer exact. However, one can generalize it heuristically as follows. We consider that action potentials are fired whenever z crosses (from below) some threshold, z_t. Then z is immediately reset to a value z_r and it evolves again according to equation B.12.

The two phenomenological parameters, z_t and z_r, cannot be determined by the exact reduction method detailed above. Instead, we estimate them by requiring that the $f - I$ curve fits the $f - I$ curve of the full model as well as possible.

Appendix C: A Measure for the Synchrony Level

To characterize the degree of synchrony in a population of N neurons in the simulations, we measure the temporal fluctuations of the membrane potential averaged over the population (Hansel & Sompolinsky, 1992; Golomb & Rinzel, 1993, 1994; Ginzburg & Sompolinsky, 1994). The quantity

$$V(t) = \frac{1}{N}\sum_{i=1}^{N} V_i(t) \tag{C.1}$$

is evaluated over time, and the variance $\sigma_V^2 = \langle [V(t)]^2\rangle_t - [\langle V(t)\rangle_t]^2$ of its temporal fluctuations is computed where $\langle \ldots \rangle_t$ denotes time averaging. After normalization of σ_V to the average over the population of the single cell membrane potentials $\sigma_{V_i}^2 = \langle\, [V_i(t)]^2\rangle_t - [\langle V_i(t)\rangle_t]^2$, one defines $\chi(N)$,

$$\chi\,(N) = \frac{\sigma_V^2}{\frac{1}{N}\sum_{i=1}^{N}\sigma_{V_i}^2}, \tag{C.2}$$

which is between 0 and 1. The central limit theorem implies that in the limit, $N \to \infty$ $\chi(N)$ behaves as

$$\chi\,(N) = \chi\,(\infty) + \frac{a}{N} + O\left(\frac{1}{N}\right), \tag{C.3}$$

where $a > 0$ is a constant. In particular, $\chi(N) = 1$, if the system is fully synchronized (i.e., $V_i(t) = V(t)$ for all i), and $\chi\,(N) = O(1/N)$ if the state of the system is asynchronous. In the asynchronous state, $\chi(\infty) = 0$. More generally, the larger $\chi(\infty) > 0$, the more the population is synchronized. In networks with more than one population of neurons, we define a synchrony measure χ for each population separately.

Acknowledgments

This work was partially supported by ECOS. The work of G.M. was partially supported by grant PICT97 03-00000-00131 from ANPCyT and by Fundación Antorchas. Fruitful discussions with N. Brunel, B. Ermentrout, D. Golomb, H. Sompolinsky, and C. van Vreeswijk are acknowledged. We thank N. Brunel, D. Golomb, and C. Meunier for careful and critical reading of the manuscript.

References

Abbott, L. F., & van Vreeswijk, C. (1993). Asynchronous state in networks of pulse-coupled oscillators. *Phys. Rev.*, *E48*, 1483–1490.

Abeles, M. (1990). *Corticonics: Neural circuits of the cerebral cortex*. Cambridge: Cambridge University Press.

Ben Yshai, R., Hansel, D., & Sompolinsky, H. (1997). Traveling waves and processing of weakly tuned inputs in cortical module. *J. Comput. Neurosci.*, *4*, 57–77.

Bergman, H., Feingold, A., Nini, A., Raz, A., Slovin, H., Abeles, M., & Vaadia E. (1998). Physiological aspects of information processing in the basal ganglia of normal and parkinsonian primates. *Trends in Neuroscience*, *21*, 32–38.

Bressloff, P. C., & Coombes, S. (2000). Dynamics of strongly-coupled spiking neurons. *Neural Comput.*, *12*, 91–129.

Brunel, N. (2000). Dynamics of sparsely connected networks of excitatory and inhibitory spiking neurons. *J. Comput. Neurosci.*, *8*, 183–208.

Brunel, N., & Hakim, V. (1999). Fast global oscillations in networks of integrate-and-fire neurons with low firing rates. *Neural Comput.*, *11*, 1621–1671.

Brunel, N., & Hansel, D. (2002). *How noise affects synchronization in recurrent networks of inhibitory neurons.* Unpublished manuscript.

Bush, P., & Sejnowski, T. (1996). Inhibition synchronizes sparsely connected cortical neurons within and between columns of realistic network models. *J. Comput. Neurosci.*, *3*, 91–110.

Buzsáki, G., & Chrobak, J. J. (1995). Temporal structure in spatially organized neuronal ensembles: A role for interneuron networks. *Curr. Opin. Neurobiol.*, *5*, 504–510.

Chow, C. C. (1998). Phase-locking in weakly heterogeneous neuronal networks. *Physica*, *D118*, 343–370.

Chow, C. C., White, J. A., Ritt, J., & Kopell, N. (1998). Frequency control in synchronized networks of inhibitory neurons. *J. Comput. Neurosci.*, *5*, 407–420.

Crook, S. M., Ermentrout, G. B., & Bower, J. M. (1998). Spike frequency adaptation affects the synchronization properties of networks of cortical oscillators. *Neural Comput.*, *10*, 837–854.

Ermentrout, G. B. (1994). Reduction of conductance based models with slow synapses to neural nets. *Neural Comput.*, *6*, 679–695.

Ermentrout, G. B. (1996). Type I membranes, phase resetting curves, and synchrony. *Neural Comput., 8*, 979–1001.

Ermentrout, G. B., & Kopell, N. (1986). Parabolic bursting in an excitable system coupled with a slow oscillation. *SIAM J. Appl. Math., 46*, 233–253.

Fuhrman, G., Markram, H., & Tsodyks, M. (2002). Spike frequency adaptation and neocortical rhythms. *J. Neurophysiol., 88*, 761–770.

Gerstner, W. (2000). Population dynamics of spiking neurons: Fast transients, asynchronous state, and locking. *Neural Comput., 12*, 43–89.

Gerstner, W., & van Hemmen, J. L. (1993). Coherence and incoherence in a globally coupled ensemble of pulse-emitting units. *Phys. Rev. Lett., 71*, 312–315.

Ginzburg, I., & Sompolinsky, H. (1994). Theory of correlations in stochastic neuronal networks. *Phys. Rev., E50*, 3171–3191.

Golomb, D. (1998). Models of neuronal transient synchrony during propagation of activity through neocortical circuitry. *J. Neurophysiol., 79*, 1–12.

Golomb, D., & Ermentrout, G. B. (1999). Continuous and lurching traveling pulses in neuronal networks with delay and spatially decaying connectivity. *Proc. Natl. Acad. Sci. USA. 96*, 13480–13485.

Golomb, D., & Hansel, D. (2000). The number of synaptic inputs and the synchrony of large sparse neuronal networks. *Neural Comput., 12*, 1095–1139.

Golomb, D., Hansel, D., & Mato, G. (2001). Theory of synchrony of neuronal activity. In S. Gielen & F. Moss (Eds.), *Handbook of biological physics*. Amsterdam: Elsevier.

Golomb, D., & Rinzel, J. (1993). Dynamics of globally coupled inhibitory neurons with heterogeneity. *Phys. Rev., E48*, 4810–4814.

Golomb, D., & Rinzel, J. (1994). Clustering in globally coupled inhibitory neurons. *Physica, D72*, 259–282.

Gupta, A., Wang, Y., & Markram, H. (2000). Organizing principles for a diversity of GABAergic interneurons and synapses in the neocortex. *Science, 287*, 273–278.

Hansel, D., & Mato, G. (2001). Existence and stability of persistent states in large neuronal networks. *Phys. Rev. Lett., 86*, 4175–4178.

Hansel, D., Mato, G., & Meunier, C. (1993a). Phase dynamics for weakly coupled Hodgkin-Huxley neurons. *Europhys. Lett., 23*, 367–372.

Hansel, D., Mato, G., & Meunier, C. (1993b). Phase reduction and neural modeling. in functional analysis of the brain based on multiple-site recordings. *Concepts in Neuroscience, 4*, 192–210.

Hansel, D., Mato, G., & Meunier, C. (1995). Synchrony in excitatory neural networks. *Neural Comput., 7*, 307–337.

Hansel, D., Mato, G., Neltner, L., & Meunier, C. (1998). On numerical simulations of integrate-and-fire neural networks. *Neural Comput., 10*, 467–483.

Hansel, D., & Sompolinsky, H. (1992). Synchrony and computation in a chaotic neural network. *Phys. Rev. Lett., 68*, 718–721.

Hansel, D., & Sompolinsky, H. (1996). Chaos and synchrony in a model of hypercolumn in visual cortex. *J. Comput. Neurosci., 3*, 7–34.

Hansel, D., & Sompolinsky, H. (1998) Modeling feature selectivity in local cortical circuits. In C. Koch & I. Segev. (Eds.), Methods in neuronal modeling: from ions to networks. Cambridge, MA: MIT Press.

Hebb, D. (1949). *The organization of behavior*. New York: Wiley.
Jefferys, J. G. R., Traub, R. D., & Whittington, M. A. (1996). Neuronal networks for induced "40 Hz" rhythms. *Trends Neurosci., 19*, 202–208.
Kuramoto, Y. (1984). *Chemical oscillations, waves and turbulence*. New York: Springer-Verlag.
Kuznetsov, Y. (1998). *Elements of applied bifurcation theory* (2nd ed.). New York: Springer-Verlag.
Latham, P. E., Richmond, B. J., Nelson, P. G., & Nirenberg, S. (2000). Intrinsic dynamics in neuronal networks. I. Theory. *J. Neurophysiol., 83*, 808–827.
McCormick, D. A., & Contreras, D. (2001). On the cellular and network bases of epileptic seizures. *Annu. Rev. Physiol., 64*, 815–846.
Neltner, L., Hansel, D., Mato, G., & Meunier, C. (2000). Synchrony in heterogeneous networks of spiking neurons. *Neural Comput., 12*, 1607–1641.
Rall, W. (1967). Distinguishing theoretical synaptic potentials computed for different some-dendritic distribution of synaptic input. *J. Neurophysiol., 30*, 1138–1168.
Rubin, N., & Sompolinsky, H. (1989). Neural networks with low local firing rates. *Europhys. Lett., 10*, 465–470.
Shelley, M. J., & Tao, L. (2001). Efficient and accurate time-stepping schemes for integrate-and-fire neuronal networks. *J. Comput. Neurosci., 11*, 111–119.
Sik, A., Penttonen, M., Ylinen, A., & Buzsáki G. (1995). Hippocampal CA1 interneurons: An in vivo intracellular labeling study. *J. Neurosci., 15*, 6651–6665.
Strogatz, H. S. (2000). *Nonlinear dynamics and chaos*. Cambridge: Perseus.
Tarczy-Hornoch, K., Martin, K. A., Jack J. J., & Stratford K. J. (1998). Synaptic interactions between smooth and spiny neurones in layer 4 of cat visual cortex in vitro. *J. Physiol., 508*, 351–363.
Traub, R. D., Jefferys, J. G., & Whittington, M. A. (1997). Simulation of gamma rhythms in networks of interneurons and pyramidal cells. *J. Comput. Neurosci., 4*, 141–150.
Traub, R. D., Jefferys, J. G. R., & Whittington, M. A. (1999). *Fast oscillations in cortical circuits*. Cambridge, MA: MIT Press.
Traub, R. D., Whittington, M. A., Colling, S. B, Buzsáki, G., & Jefferys, J. G. R. (1996). Analysis of gamma rhythms in the rat hippocampus in vitro and in vivo. *J. Physiol. (London), 493*, 471–484.
Treves, A. (1993). Mean field analysis of neuronal spike dynamics. *Network, 4*, 259–284.
Tsodyks, M. V., Skaggs, W. E., Sejnowski, T. J., & McNaughton B. L. (1997). Paradoxical effects of external modulation of inhibitory interneurons. *J. Neurosci., 17*, 4382–4388.
van Vreeswijk, C. (1996). Partial synchronization in populations of pulse-coupled oscillators. *Phys. Rev., E54*, 5522–5537.
van Vreeswijk, C. (2000). Analysis of the asynchronous state in networks of strongly coupled oscillators. *Phys. Rev. Lett., 84*, 5110–5113.
van Vreeswijk, C., Abbott, L. F., & Ermentrout, G. B. (1994). When inhibition not excitation synchronizes neural firing. *J. Comput. Neurosci., 1*, 313–321.
van Vreeswijk, C., & Hansel, D. (2001). Patterns of synchrony in neural networks with adaptation. *Neural Comput., 13*, 959–992.

van Vreeswijk, C., & Sompolinsky, H. (1996). Chaos in neuronal networks with balanced excitatory and inhibitory activity. *Science, 274*, 1724–1726.
van Vreeswijk, C., & Sompolinsky, H. (1998). Chaotic balanced state in a model of cortical circuits. *Neural Comput., 10*, 1321–1372.
Wang, X.-J. (1999). Synaptic basis of cortical persistent activity: The importance of NMDA receptors to working memory. *J. Neurosci., 19*, 9587–9603.
Wang, X.-J., & Buzsáki, G. (1996). Gamma oscillation by synaptic inhibition in a hippocampal interneuronal network model. *J. Neurosci., 16*, 6402–6413.
Wang, X.-J., & Rinzel, J. (1992). Alternating and synchronous rhythms in reciprocally inhibitory model neurons. *Neural Comput., 4*, 84–97.
White, J. A., Chow, C. C., Ritt, J., Soto-Treviño, C., & Kopell, N. (1998). Synchronization and oscillatory dynamics in heterogeneous, mutually inhibited neurons. *J. Comput. Neurosci., 5*, 5–16.
Whittington, M. A., Traub, R. D., & Jefferys, J. G. R. (1995). Synchronized oscillations in interneuron networks driven by metabotropic glutamate receptor activation. *Nature, 373*, 612–615.
Whittington, M. A., Traub, R. D., Kopell, N., Ermentrout, B., & Buhl, E. H. (2000). Inhibition-based rhythms: Experimental and mathematical observations on network dynamics. *Int. J. of Psychophysiology, 38*, 315–336.

Received April 25, 2002; accepted June 27, 2002.